Direct Evaluation of T_ε^* Integral from Experimentally Measured Near Tip Displacement Field, for a Plate with Stably Propagating Crack

H. Okada and S. N. Atluri

Computational Mechanics Center
Georgia Institute of Technology
Atlanta, GA 30332-0356

ABSTRACT

In this paper, a method to quantitatively evaluate the T_ε^* integral directly from the measured near-tip displacement field for laboratory specimens made of metallic materials, is presented. This is the first time that such an attempt became a success. In order to develop the procedure, we carefully examine the nature of T_ε^*. Hence, the nature of T_ε^* is further revealed. Following Okada and Atluri (1997), the relationship between energy balance statements for a cracked plate and the T_ε^* is discussed. It is concluded that T_ε^* quantifies the deformation energy dissipated near crack tip region [an elongating strip of height ε] per unit crack extension. In the evaluation of T_ε^* integral directly from measured displacement field, the use of deformation theory plasticity (J2-D theory) and the truncation of the near crack integral path on the experimental studies of Omori et el. (1995) are presented, and these show a good agreement with the results of finite element analysis.

DISCLAIMER

DISCLAIMER

Portions of this document may be illegible in electronic image products. Images are produced from the best available original document.

1 Introduction

The T_ε^* integral was developed by Atluri, Nishioka and Nakagaki (1984) and it has been known that the T_ε^* is a very useful fracture parameter [see Brust (1984), Brust et al. (1986), Nishioka et al. (1992), Newman et al. (1993), Okada et al. (1992), Pyo et al. (1995), Toi et al. (1990a, 1990b, 1990c), Wang et al. (1997a, 1997, 1997c)]. T_ε^* has been applied to characterize the crack tip field, during stable crack growth, of ductile as well as brittle materials. The use of T_ε^* is not limited to elastic (general nonlinear elastic) materials unlike the J integral (in theory, the use of J integral is limited to (nonlinear) elastic materials [Rice (1968)]). However, T_ε^* is not yet fully utilized in the fracture analysis of practical elastic-plastic problems. The reasons for this may lie in the difficulties in the direct experimental measurement of the T_ε^* integral from laboratory specimens. It always involved a support of numerical analysis (Finite Element Method). The series of recent research efforts by the authors [Okada et al. (1995) and Omori et al. (1995) and this paper] may alleviate such difficulties in the use of T_ε^* and may make it possible to utilize T_ε^* for practical purposes. Especially in Okada and Atluri (1997), the relationship between T_ε^* and CTOA (crack tip opening angle) in the case of stably growing crack in ductile material, has been clarified. As shown in Okada and Atluri (1997), the $T_\varepsilon^*\big|_{Elongating}$, for low hardening materials with steady-state crack growth, is roughly equal to the energy deposited in the wake of height ε behind the advancing crack-tip, for unit of crack extension. Thus, it has a physical basis for characterizing stable crack growth.

In this paper, we discuss a procedure for the determination of the T_ε^* integral from experimentally measured surface displacement data near the crack-tip in a plate. Difficulties in such attempts lie in the determination of the stresses. The experimentally measured displacements are, in general, desecrate data with respect to time. In the case of metallic materials, it is quite difficult to determine stresses, due to lack of complete information on the deformation history. In general, the determination of stresses for ductile material requires a complete information on strain history. The stresses and workdensity, which are necessary in the T_ε^* evaluation, may be very erroneous, if such information is not complete. Hence the calculated T_ε^* integral value may involve an unacceptably large error.

Yagawa et al (1992) and Nishioka (1992) have dealt with such challenging issues. Yagawa et al. (1992) disregarded the integral path far behind the crack tip and used deformation theory of plasticity (J2-D theory). And they concluded that the neglection of a part of integral path behind the advancing crack tip, resulted in a increase-decrease-level behavior during stable crack growth. Nishioka et al. (1992) attempted to take correlations between the size of caustic zone and T_ε^* value.

The earlier part of present course of study [Okada and Atluri (1997)] further revealed the properties and nature of the T_ε^* as a crack tip parameter for stable crack growth in metallic materials. It has been concluded that, for stale crack growth in metallic (ductile) material, the $T_\varepsilon^*|_{Elongating}$ quantifies the energy dissipated inside the extending strip of height ε [the size of the path $T_\varepsilon^*|_{Elongating}$], per unit crack extension. For low hardening materials, energy release rate at the crack tip was concluded to be nearly zero.

Based on the earlier studies of Okada and Atluri (1997), we further examine the nature of the T_ε^* integral. This leads to a useful method to evaluate the T_ε^* integral directly from experimentally measured displacement field. Use of the deformation theory plasticity (J2-D theory) and the truncation of the near crack integral path just behind the crack tip are suggested. Some results based on the experimental studies of Omori et al. (1995) are presented. In section 2, discussions on the definition of the T_ε^* integral and T_ε^* as a fracture parameter, are given. In section 3, based on the discussions and conclusions in section 2, a methodology to calculate T_ε^* directly from measured displacement data, is proposed. In section 4, the results of T_ε^* evaluation are presented. Due to the developments presented in this paper, it now becomes possible to quantitatively evaluate T_ε^* directly from experimental data.

The present study is followed by Omori et al. (1995) to analyze stable crack growth in SEN fracture specimens made of aluminum alloy 2024T3 and of high strength steel A606.

2. Definition of the T_ε^* Integral and T_ε^* as a Fracture Toughness Parameter

2-1. Implications of Near tip Contour Integral T_ε^* on Different (Elongating and Moving) contour paths

The energy flows per unit crack extension from the rest of the cracked solid in to a volume V_ε that is enclosed by a small contour Γ_ε of size ε, centered at the moving crack tip (for arbitrary size ε) is given by,

$$\underset{\Delta a \to 0}{Lt}\left(\frac{\Delta E_{\Gamma_\varepsilon}}{\Delta a}\right) = \int_{\Gamma_\varepsilon} t_i \frac{Du_i}{Da} ds + \int_{V_\varepsilon} f_i \frac{Du_i}{Da} dv - \frac{D}{Da}\int_{V_\varepsilon} (W + T) dv \qquad (1)$$

where ε is small but finite. Equation (1) is valid for any type (i.e., not necessarily elastic) material behavior, and Γ_ε is a contour of arbitrary size, instantaneously centered at the moving crack-tip as shown in Figure 1, and Δa is the size of crack growth increment.

Restricting our attention to quasi-static steady state crack growth, following the argument presented in [Atluri (1986) and Atluri (1997)], we can write equation (1), as:

$$\underset{\Delta a \to 0}{Lt}\left(\frac{\Delta E_{\Gamma_\varepsilon}}{\Delta a}\right) = \int_{\Gamma_\varepsilon}\left(Wn_1 - t_i\frac{\partial u_i}{\partial x_1}\right)ds - \int_{V_\varepsilon}\left(\frac{\partial W}{\partial a} - f\frac{\partial u_i}{\partial a} + f_i\frac{\partial u_i}{\partial x_1}\right)dv + \int_{\Gamma_\varepsilon}\left(t_i\frac{\partial u_i}{\partial a}\right)ds \quad (2)$$

We consider that the magnitude of ε is such that $\varepsilon > \Delta a$.

Consider steady state conditions near the crack-tip, i.e., consider that stage of propagation of the crack in a finite elastic-plastic body where, at least very near the crack-tip, the stress, strain and displacement fields are invariant. Thus, if (ξ_1, ξ_2) is a coordinate system centered at the moving crack tip, such that

$$\xi_1 = x_1 - a \quad (3)$$

where a is the changing coordinate of the crack-tip in the space-fixed coordinate system x_1, and if steady-state conditions are reached at least near the crack-tip, we have:

$$\left.\frac{\partial(\ )}{\partial a}\right|_{\xi_1} = 0 \qquad \text{in } V_\varepsilon. \quad (4)$$

Thus, under steady-state conditions in V_ε and when $f_i = 0$, we have:

$$\underset{\Delta a \to 0}{Lt}\left(\frac{\Delta E_{\Gamma_\varepsilon}}{\Delta a}\right) = T_\varepsilon^*\Big|_{Moving} \equiv \int_{\Gamma_\varepsilon|_{Moving}}\left(Wn_1 - t_i\frac{\partial u_i}{\partial x_1}\right)ds \quad (5)$$

We consider that the magnitude of ε is such that $\varepsilon > \Delta a$.
Consider a low-hardening elastic-plastic material wherein the stress saturates to a finite value near the crack-tip. In this case, the crack-tip cohesive tensions, which are non-singular, do zero work in the limit as $\Delta a \to 0$, while in the linear elastic case where the crack-tip tractions are of $r^{-\frac{1}{2}}$ type and do non-zero work in undergoing a crack-opening displacement of the type $r^{\frac{1}{2}}$ even in the limit as $\Delta a \to 0$. Thus, in the low-hardening elastic-plastic case, in the limit as $\varepsilon \to 0$, the total energy ΔE that is fed from the surrounding solid into the crack-tip region is entirely spent in extending the wake by Δa, and in the limit as $\Delta a \to 0$, tends to zero. Thus, $\underset{\varepsilon \to 0}{Lt}\, T_\varepsilon^*\big|_{Moving} \to 0$ during crack growth.

However, for a finite value of ε, the energy that is fed into Γ_ε tends to be finite, even as $\Delta a \to 0$, since this energy goes not only into opening the crack, but is also dissipated as plastic work within Γ_ε.

The definition of the path Γ_ε can be changed to consider not only the loading zone ahead of the propagating crack-tip, but also the wake zone in Figure 2. Figure 2 (a) shows the elongating Γ_ε contour path; while Figure 2 (b) shows moving Γ_ε contour even for the elongating Γ_ε, if steady state conditions prevail near the crack-tip and in the wake, we have:

$$\underset{\Delta a \to 0}{Lt}\left(\frac{\Delta E_{\Gamma_\varepsilon}}{\Delta a}\right) = T_\varepsilon^*\Big|_{Elongating} = \int_{\Gamma_\varepsilon|_{Elongating}}\left(Wn_1 - t_i\frac{\partial u_i}{\partial x_1}\right)\mathrm{d}s \tag{6}$$

where, $\Delta E_{\Gamma_\varepsilon}$ is the total of (i) deformation energy dissipated inside the elongating contour Γ_ε, as well as (ii) the energy spent in opening the crack by an amount Δa. It is thus seen, under steady-state conditions,

$$T_\varepsilon^*\Big|_{Elongating} >> T_\varepsilon^*\Big|_{Moving} \qquad \text{for any finite value of } \varepsilon. \tag{7}$$

In both (5) and (6), for an elastic-plastic solids, W is the stress-work density:

$$W = \int_0^{\varepsilon_t} \sigma_{ij}\,\mathrm{d}\bar{\varepsilon}_{ij} \tag{8}$$

It is noted that equations (5), (6) and (8) are written for the case of infinitesimal deformations.

From equations (5) and (6), one may write under steady-state conditions:

$$T_\varepsilon^*\Big|_{Elongating} = \frac{D}{Da}\int_{V_\varepsilon} W\,\mathrm{d}v + \frac{DE_{Crack}}{Da} \qquad : \Delta a \to 0,\ \varepsilon \text{ finite.} \tag{9}$$

where E_{Crack} is the energy dissipated due to the creation of new crack surfaces.

On the other hand, $T_\varepsilon^*\Big|_{Moving}$ measures the energy needed to create new crack surfaces, per unit crack propagation. On may write:

$$T_\varepsilon^*\Big|_{Moving} = \frac{DE_{Crack}}{Da} \tag{10}$$

From equations (3) and (4), one may relate $T_\varepsilon^*\Big|_{Elongating}$ and $T_\varepsilon^*\Big|_{Moving}$ by the following equation.

$$T_\varepsilon^*\Big|_{Elongating} = \frac{D}{Da}\int_{V_\varepsilon} W\,\mathrm{d}v + T_\varepsilon^*\Big|_{Moving} \tag{11}$$

For a ductile material, the deformation energy dissipated in the region inside Γ_ε dominates that for creating new crack surfaces. Therefore, one may write:

$$\frac{D}{Da}\int_{A_\varepsilon} W \, dA_\varepsilon >> \frac{DE_{Crack}}{Da} \tag{12}$$

Thus, as stated in equation (7).

$$T_\varepsilon^*\Big|_{Elongating} >> T_\varepsilon^*\Big|_{Moving} \tag{13}$$

For the steady state, the deformation energy dissipated inside the elongating Γ_ε contour, can be measured by a line integral on a vertical line from the crack face (line) inside wake zone (see also Figure 3).

$$\frac{D}{Da}\int_{A_\varepsilon} W \, dA_\varepsilon = 2\int_0^\varepsilon W \, dx_2 \qquad \text{(in wake zone)} \tag{14}$$

Equation (14) is valid only for the case of steady state crack propagation, under an assumption that most of deformation energy is attributed to plastic energy dissipation. Elastic part of workdensity does not play a major role.

Both $T_\varepsilon^*\big|_{Elongating}$ and $T_\varepsilon^*\big|_{Moving}$ are closely related with the near crack tip deformation field and can be good crack tip parameters. It should, however, be pointed out here that, because $T_\varepsilon^*\big|_{Moving}$ is far smaller than $T_\varepsilon^*\big|_{Elongating}$, $T_\varepsilon^*\big|_{Elongating}$ may be much easier to calculate without the influences of error associated with any numerical computations.

From the above discussions, we can draw conclusions:

- The $T_\varepsilon^*\big|_{Elongating}$ integral represents amount of energy dissipated in the region inside the Γ_ε contour path, per unit of crack extension.
- The T_ε^* integral, in turn, can be seen as material resistance to crack propagation. Therefore, $\left(T_\varepsilon^*\big|_{elongating}\right)_{Applied} = \left(T_\varepsilon^*\big|_{elongating}\right)_{Resistance}$ is a criterion for stable crack growth, and $\left(T_\varepsilon^*\big|_{elongating}\right)_{Applied} > \left(T_\varepsilon^*\big|_{elongating}\right)_{Resistance}$ signifies loss of stability and the initiation of unstable crack propagation.

3. Procedures for Experimental Evaluation of the T_ε^* Integral

Recently, several attempts to evaluate the T_ε^* integral directly from experimentally measured displacements or caustic zone size, have been made. [see Nishioka et al. (1992) for caustic zone size, Yagawa et al. (1992) and Omori et al. (1995) from measured surface displacements]. In the present investigation, we attempt to calculate the integral parameter, from the surface displacements measured by moiré interferometry. Stable crack propagation experiments for 2024T3 and A606 high strength steel were conducted at the fracture mechanics laboratory of A.S. Kobayashi at the University of Washington.

There are several important issues to resolve in the current attempt. The first is that, the stresses and workdensity which are necessary to calculate the integral parameter, are not directly measured in the experiment. Hence, we have to assume a constitutive equation to evaluate those quantities. The second is that the experimental data can not give a complete information of the deformation history. This means that one may use an incremental theory of plasticity, but it may be erroneous, especially when the elastic unloading phenomenon is incorporated.

In this section, some inherent problems associated with the evaluation of T_ε^* integral directly from the experimentally measured displacement data will be discussed. They are: 1) approximate methods to calculate the stresses and workdensity, and 2) approximate method to evaluate the T_ε^* integral.

3-1 Approximate Method to Calculate the Stresses and Workdensity

In general, a complete deformation history at a material point is not available in experimental measurement. The stresses and work density are not available too. We need to calculate the stresses based on the given displacement field. Though one can calculate the current state of strains, that is not enough information to evaluate the stresses correctly.

In the present course of study the deformation theory plasticity (J2 Deformation Plasticity: J2-D) is adopted to calculate stresses from given strains. The relationship between the stresses and strains are written to be:

$$\varepsilon_{ij} = \frac{1-\nu}{E}\sigma_{mm}\delta_{ij} + \frac{1}{2G}\sigma'_{ij} + \chi\sigma'_{ij}, \quad \chi = \frac{3}{2}\frac{\bar{\varepsilon}^P}{\bar{\sigma}}, \quad \bar{\varepsilon}^P = \left(\frac{3}{2}\varepsilon^P_{ij}\varepsilon^P_{ij}\right)^{\frac{1}{2}}, \quad \bar{\sigma} = \left(\frac{2}{3}\sigma'_{ij}\sigma'_{ij}\right)^{\frac{1}{2}} \quad \text{...(1)}$$

Since, stresses σ_{ij} and plastic strains ε^P_{ij} are initially unknown, they are calculated through an iteration algorithm.

Under proportional loading, the stresses calculated by the J2-D theory is identical to those calculated by the J2 flow (incremental plasticity: J2-F) theory. The results of J2-D and J2-F are especially different from each other when elastic unloading occurred. J2-D theory can not correctly represent such deformation history.

Once the stresses are determined, then the workdensity is calculated by its definition.

3-2 Method to Calculate the T_ε^* Integral from Experimentally Measured Displacement Data.

In this section, procedures of the T_ε^* integral evaluation from experimentally measured displacement data, are discussed.

The displacement field recorded by the moiré interferometry method is reduced to pointwise numerical data at grid points. The schematics of the grid is shown in Figure 4.
Then, the finite element type by-linear local interpolation functions are introduced to numerically differentiate the displacement field, and then strains are obtained. Stresses and workdensity are evaluated based on the J2-D plasticity theory as described in section 3-1.

The equivalent domain integral (EDI) method Nikishkov and Atluri (1987) is employed to carry out the T_ε^* integral computation. In the EDI method the contour integral on Γ_ε path is converted to an area integral by introducing "S" function. "S" function takes 1 and 0, on Γ_ε path and on outer contour Γ, respectively. The EDI method is schematically described in Figure 5.

However, the above procedures with the experimentally measured displacement field involve the following problems. And they are the crux of the present research.

- Due to a lack of a complete strain (deformation) history information, the stresses and workdensity behind the crack tip (say in the wake zone) is especially erroneous.
- Here, the T_ε^* integral values are overestimated. When the "elongating" Γ_ε path is used, the value keeps increasing as the crack extends (see Figure 6). This is because the integral area in EDI method keeps increasing. When the "moving" Γ_ε path is used, the T_ε^* integral value may be incorrect also. This is because, in the wake zone, the stresses and workdensity are NOT evaluated correctly.

In the following sections, we seek (a) way(s) to circumvent the above stated problems in the experimental T_ε^* integral evaluation. We first discuss the nature of the T_ε^* integral further, and propose a method to circumvent the problems. Then, the proposed methodologies are verified by some numerical experiments, in which the T_ε^* integral are evaluated from the Finite Element Displacement data.

3-3. An Approximate Method to Calculate T_ε^* from Experimentally Measured Displacement Data

In this section, we investigate the nature of the integral parameter further. We are mainly concerned with the contribution of each segment of Γ_ε contour path. Hence, we examine which segments of Γ_ε have significant contributions to the integral, and also which segments have negligible contribution. If the part of the Γ_ε integral contour, which is associated with the problems pointed out in sections 3-1 and 3-2, were essentially negligible, we simply disregard that part of the contour. Through an investigation presented in this section, we find that the contribution form the path behind the crack tip (which is troublesome) is small. Hence we disregard that part from the integral.

First, we consider the distribution of stress along the contour. As seen in Figure 7 (a), we can assume that in the vicinity of the crack face, that σ_{12} and σ_{22} are nearly zero, because they are zero at the crack face. Hence, we can assume that on the segments B-C and F-G in the Γ_ε contour path, as (points C and F are just behind the crack tip):

$$\sigma_{12} \approx 0, \qquad \sigma_{22} \approx 0 \qquad \text{on B-C and F-G} \tag{12}$$

On the other hand, on segments B-C and F-G, stress σ_{11} is non-zero, because this is residual stress in the wake zone.

Also, on segments B-C and F-G, the x_1 direction component of the unit outward normal vector n_1^ε is zero. Hence, we can conclude that the contribution of these segments to the T_ε^* integral value is small.

$$\int_{\Gamma_\varepsilon(B-C,F-G)} \left(W n_1^\varepsilon - n_i^\varepsilon \sigma_{ij} \frac{\partial u_j}{\partial x_1} \right) d\Gamma_\varepsilon = \int_{\Gamma_\varepsilon(B-C,F-G)} \left(-n_2^\varepsilon \sigma_{2j} \frac{\partial u_j}{\partial x_1} \right) d\Gamma_\varepsilon \approx 0 \tag{13}$$

Let us consider the segments of the Γ_ε path just behind the original crack tip, namely A-B and G-H. This part of the material never experienced severe stress concentration and remains to be elastic. Therefore, the workdensity there, is considered to be small. Also, this part is far away from the current crack tip and no plastic deformation (no residual stress due to plastic deformation). Thus stresses, also, are very small. hence, one can write:

$$\int_{\Gamma_\varepsilon(A-B,G-H)} \left(W n_1^\varepsilon - n_i^\varepsilon \sigma_{ij} \frac{\partial u_j}{\partial x_1} \right) d\Gamma_\varepsilon \approx 0 \tag{14}$$

It is noted that, in the section 2 [equations (9) and (10)], the term $\int_{\Gamma_\varepsilon(A-B,G-H)} W n_1^\varepsilon d\Gamma_\varepsilon$ is not included in the expression for energy dissipation inside the Γ_ε integral contour. It also suggests the exclusion of the term $\int_{\Gamma_\varepsilon(A-B,G-H)} W n_1^\varepsilon d\Gamma_\varepsilon$.

Thus, we can write, that to a good approximation,

$$T_\varepsilon^* = \int_{\Gamma_\varepsilon}\left(Wn_1^\varepsilon - n_i^\varepsilon\sigma_{ij}\frac{\partial u_j}{\partial x_1}\right)\mathrm{d}\Gamma_\varepsilon$$

$$= \int_{\Gamma_\varepsilon(C-D-E-F)}\left(Wn_1^\varepsilon - n_i^\varepsilon\sigma_{ij}\frac{\partial u_j}{\partial x_1}\right)\mathrm{d}\Gamma_\varepsilon = \int_{\Gamma_\varepsilon(D-E)}Wn_1^\varepsilon\mathrm{d}\Gamma_\varepsilon - \int_{\Gamma_\varepsilon(C-D-E-F)}n_i^\varepsilon\sigma_{ij}\frac{\partial u_j}{\partial x_1}\mathrm{d}\Gamma_\varepsilon \quad ...(15)$$

We can see in equation (15) that the T_ε^* integral can approximately be evaluated by the integration only on C-D-E-F. We designate this path as the "***Cut-off***" integral path.

Let us consider the evaluation of the T_ε^* integral using the "Equivalent Domain Integral (EDI) Method" based on equation (15). We introduce a function *S(x)*, where ***x*** is the coordinate of a material point, such that, on the segment C-D-E-F of Γ_ε, *S(x)*=1, and on C'-D'-E'-F' on the outer contour Γ, *S(x)*=0. The outer contour G is shown in Figure 7 (a). And we assume that segments C'-D' and E'-F' are parallel to C-D and E-F, respectively. We shall let *S(x)* such that, in the region between segments the C-D and C'-D' and between E-F and E'-F', *S(x)* does not vary in x_1 direction. In the other words, *S(x)* is only a function of x_2, as shown in Figure 7 (a).

By applying the Gauss divergence theorem, we have:

$$T_\varepsilon^* = \int_{\Gamma_\varepsilon(C-D-E-F)}\left(Wn_1^\varepsilon - n_i^\varepsilon\sigma_{ij}\frac{\partial u_j}{\partial x_1}\right)\mathrm{d}\Gamma_\varepsilon$$

$$= \int_{\Gamma_\varepsilon(C-D-E-F)}\left(S(x)Wn_1^\varepsilon - S(x)n_i^\varepsilon\sigma_{ij}\frac{\partial u_j}{\partial x_1}\right)\mathrm{d}\Gamma_\varepsilon$$

$$= -\int_A\left(\frac{\partial S(x)W}{\partial x_1} - \frac{\partial S(x)\sigma_{ij}\frac{\partial u_j}{\partial x_1}}{\partial x_1}\right)\mathrm{d}A + \int_{\Gamma_\varepsilon(C-C',F'-F)}\left(S(x)W\bar{n}_1 - S(x)\bar{n}_i\,\sigma_{ij}\frac{\partial u_j}{\partial x_1}\right)$$

$$= -\int_A\left(\frac{\partial S(x)W}{\partial x_1} - \frac{\partial S(x)\sigma_{ij}\frac{\partial u_j}{\partial x_1}}{\partial x_1}\right)\mathrm{d}A + \int_{\Gamma_\varepsilon(C-C',F'-F)}\left(-S(x)W + S(x)\sigma_{1j}\frac{\partial u_j}{\partial x_1}\right) \quad ...(16)$$

where $\bar{n}$ is unit outward normal vector on segments C-C' and F-F'.

The first term in equation (16) can be calculated by using the method of Nikishikov and Atluri (1987). The last term in equation (16) can also be evaluated approximately by using an integral in a narrow strip $\bar{A}$, whose centers are C-C' and F-F' and width is *t*. They are also depicted in Figure 7 (b).

$$\int_{\Gamma_\varepsilon(C-C',F'-F)}\left(-S(x)+S(x)\sigma_{1j}\frac{\partial u_j}{\partial x_1}\right)d\Gamma_\varepsilon$$

$$-\frac{1}{t}\int_{\overline{A}\ (C-C',F-F')}\left(-M(x_2)+M(x_2)\sigma_{1j}\frac{\partial u_j}{\partial x_1}\right)dA_{\varepsilon(C-C',F-F')} \quad (17)$$

where $M(x_2)$ is a function of x_2 and is equal to $S(\mathbf{x})$ on the segments C-C' and F-F'. In the T_ε^* integral evaluation in this course of study, the narrow strips $\overline{A}$ are set to be a band of a width of 2 elements in the finite element method, and a band of 2 grid distances in the direct evaluation from the moiré displacement data. In both the cases, the center of the band is at segments C-C' and F-F'.

From the discussions given in Section 3, we can conclude the followings:

For the T_ε^* integral evaluation, when experimentally measured displacement data is given:

- Deformation Plasticity Theory (J2-D) should be used.
- "*Cut-off*" Γ_ε integral path with modified EDI method, as described in equations (16) and (17) should be used.
- The optimum positions of the "*Cut-off*" points (say points C and F) should be small distance behind the advancing crack tip. They are yet unknown.
- Most importantly, the T_ε^* integral with "Cut-off" integral contour has the significance as the true T_ε^* showing the energy dissipated in the near crack region per unit crack extension.

4. T_ε^* Integral Evaluations from Experimental Data for Aluminum Alloy 2024T3 and for High Strength Steel A606: Numerical Experiments-the Optimum Positions of Cut-off Points C and F.

In this section, the followings are discussed.

- The optimum positions of the points C and F, which are "*Cut-off*" points of the Γ_ε integral contour for approximate evaluation of the T_ε^* integral.
- The T_ε^* integral values directly calculated from experimentally measured displacement data.

The procedures of numerical experiments are as follows.

- Finite element analysis are performed based on stable crack growth experiments of Omori et al (1995).

- T_ε^* integrals are evaluated using the results of the finite element analysis (displacements, stresses and workdensity) with *"ELONGATING"* Γ_ε and with *"Cut-off"* integral path by changing the positions of points C and F.
- T_ε^* integrals are evaluated based only on the displacement results of the finite element analysis, with *"ELONGATING"* Γ_ε and *"Cut-off"* integral path by changing the positions of points C and F.
- By comparing above two results, we discuss about the optimum position for the points C and F.

4-1 Finite Element Analysis for 2024T3 and A606 SEN Specimens

The results of the analyses and their physical implications are fully discussed in Omori et al (1995). In this section, the analysis procedures and results are briefly discussed. It is noted that the T_ε^* integral values calculated using the finite element results (stresses, workdensity and displacements) are the reference values in the following numerical experiments.

2024T3

The boundary conditions and the problem statements are given in Figure 8. Only a part of the specimen between the crack line and 10 mm above it, is modeled by the FEM. The displacement boundary conditions at y=10 mm line is given from the experimental moiré measurement. By considering the symmetry of the problem and data scatter in the experiment, the given displacements at y=10 mm line are the average of experimentally measured displacements at y=10mm and y=-10mm. The size of elements at the crack tip is 0.25 mm, and 4 node linear elements were employed. The analysis was carried out under the plane stress assumption.

The dimensional stress-plastic strain relationship is given in Figure 9. Young's modulus is 75 GPa and Poison's ration is 0.33. The J2-Flow incremental plasticity theory is employed as the constitutive low. The analysis is performed under the plane stress assumption. The crack propagation algorithm is based on the nodal release method.

A good correlation between the experiment and the Finite Element Analysis is seen in the Load-Crack Extension Curve (R-curve) [Figure 10]. The T_ε^* integrals based on the "elongating Γ_ε path" with various sizes are calculated and shown in Figure 11. As previously suggested [see Brust (1985) and Brust et al (1986)], for larger contour size, the T_ε^* integral value becomes large. But they are always smaller than the J integral value. At around crack extension 6 mm, they exhibit the steady state (the curves become flat). These can be considered as the material characteristic value of the T_ε^* integral in the steady state crack growth.

A606

In this case the whole specimen was modeled, and the displacement boundary condition at the top hole was given such that the load calculated by FEM, matches with the load measured in the experiment. Problem Statements, along with the finite element mesh are given in Figure 12. The size of elements at the crack tip is 0.5 mm, and 4 node linear elements were employed. The Young's modulus is 206 GPa and Poison's ratio is 0.295. One dimensional stress-plastic strain curve is given in Figure 13. The calculation was performed under the plane stress condition and J2-F theory was again employed.

The load-crack extension curve (R-curve) is shown in Figure 15. The T_ε^* integrals based on the "elongating Γ_ε path" with various sizes are calculated and shown in Figure 15. In this case, the steady state (constant value of the T_ε^* integrals) was not seen. This is because the degree of ductility is so large in this case that the amount of crack extension is not large enough to reach a steady state.

The plastic zone*) size at the initiation for 2024T3 and A606 are shown in Figure 16. In the case of 2024T3, it extends upto about 8.5 mm ahead the initial crack tip. This is roughly the same as or little longer than the length of crack propagation needed to reach the steady state. On the other hand, in the case of A606, the specimen experiences full ligament yielding at the crack propagation initiation. Thus, in this case, the steady state was not reached.

4-2 Optimum *Cut -Off* Positions for the *Cut-off* Integral Path

In this section, the optimum cut-off positions C and F are to be found through some numerical experiments. To emulate T_ε^* determination from experimentally measured displacement data, the finite element displacement results are used as displacement input and some comparisons are made.

The values of the T_ε^* integral, in the case of 2024T3, are compared at first. In Figure 17, the T_ε^* integral values against to the length of crack extension are plotted. The height of the Γ_ε path ε is 1.0 mm. There are three lines plotted in Figure 17. They are the cases of 1) "Elongating" Γ_ε path with Stresses and Workdensities calculated in the finite element analysis using the incremental J2-Flow theory (this one is the reference solution; correct values), 2) "Elongating" Γ_ε path with Stresses and Workdensities calculated by the deformation plasticity theory (J2-D) using displacement input and 3) "Cut-off" Γ_ε path with Stresses and Workdensities calculated by the deformation plasticity theory (J2-D) using displacement input. It is clearly seen that the case of "Elongating" Γ_ε path with J2-D theory overestimates the T_ε^* value. On the other

*) The definition of the plastic zone is the region which has non-zero plastic strain in the finite element analysis results. It may appear vary large compared with experimentally observed plastic zone size (such as based on caustic zone size).

hand, the case of "Cut-off" Γ_ε path with J2-D theory is in a good agreement with the reference values. The same observation can be made for the case that the height of the Γ_ε path ε is 2.0 mm (see Figure 18).

The relationships between the distance of cut-off points C and F from the advancing crack tip, are further investigated and are shown in Figures 19 (a), (b) and (c), for the cases of ε being 2.0 mm, 1.0 mm and 0.5 mm, respectively. The values plotted in Figures and 18 and 19 are at crack extension 8.5 mm, which is already in the steady state. Except for the case of "Elongating" Γ_ε path with J2-D plasticity theory, the integral have reached to constant values of steady state crack propagation. Comparisons are made between the cases using J2-F and J2-D plasticity theory in the stress calculations. When the cut off distance behind the crack tip is very small, both the cases result in slight underestimation. The one with J2-D plasticity theory increases as the cut-off distance become larger, where as the one with J2-F theory converges to the reference value (case of elongating path). the best case is that the positions of points C and F are 0.5 mm behind the advancing crack tip.

The same conclusion can be drawn from the analysis for A606. In Figures 20 (a), (b) and (c), the comparisons between the J2-F incremental plasticity theory and J2-D theory for different cut-off distance are drawn. Again, the J2-D with large cut-off distance results in an unacceptable overestimation. The best cut-off position seems to be at directly above and below the advancing crack tip.

From the numerical experiments, we can draw some conclusions as follows:

- By the use of *Cut-off* integral path with J2-D theory, we can characterize the stable crack growth in ductile material. The calculated T_ε^* values exhibit the plateau when the crack propagation reaches to its steady state. This means that, no matter the cut-off positions are, we can qualitatively characterize the state of crack propagation directly from experimental displacement data.
- The best cut-off position is somewhere between directly below and above the crack tip (A606) and slightly behind (0.5 mm in the case of 2024T3). This may be different for different material. In order to quantitatively evaluate T_ε^*, we need a priori knowledge of where precisely the cut-off position should be.

4-2 Evaluation of T_ε^* Integral from Experimentally Measured Displacement Data

The displacement data measured by moiré interferometry experiments are used to calculate the T_ε^* integral values. The cut-off positions of Γ_ε path are directly below and above the advancing crack tip.

<u>**2024T3**</u>

First, the results for Al alloy 2024T3 are presented. The cut-off position was set to be 0.5 mm behind the crack tip. However, since the crack position was not directly on a grid point and is always advanced than the corresponding grid point, we take an average of values using two cut-off positions. They are directly above and below the crack tip and 0.5 mm behind of it. The crack positions and their corresponding grid positions are given in Table 1. The values directly calculated from the experimental displacement data are compared with those by the Finite element method. For the case, that the height of Γ_ε path is 1.0 mm, it seems that both the values are in good agreement quantitatively after crack extension 6 mm (Figure 21).. Just after crack propagation initiation, the value from experimental displacement data are slightly higher. In the case that that the height of Γ_ε path is 2.0 mm, the same observation as the previous one can be made (see Figure 22). Nevertheless, the trends are in a complete match.

Table 1 Crack Positions and Their Corresponding Grid Position

Crack Position	Corresponding Grid Position
0 mm	0 mm
0.14 mm	0 mm
0.71 mm	0.5 mm
1.22 mm	1.0 mm
2.60 mm	2.5 mm
7.58 mm	7.5 mm
10.61 mm	10.5 mm

A606

The results for A606 high strength steel are as follows. In Figures 23 and 24, the cases of the height of Γ_ε path being 1.0 mm and 2.0 mm, respectively, are shown. In both the cases the results obtained directly from experimental displacement data, are consistently smaller than those from Finite Element Analysis results, but their trends agree.

As for the case of 2024T3, the crack tip positions are not always exactly on grid points. For A606, we took averages of two crack lengths on the grid for T_ε^* computation to compromise this problem. In Table 2, crack tip positions and their corresponding crack extension length on the grid, are shown.

As suggested in the section 4-2, the "*Cut-off*" Γ_ε path was employed with the experimental displacement data. The cut-off positions are directly above and below the crack tip.

Table 2 Crack Tip Positions and Their Corresponding Grid Positions

Crack Position	Corresponding Grid Position	
0 mm	0.0 mm	N/A
0.3 mm	0.0 mm	0.5 mm
0.5 mm	0.5 mm	N/A
0.9 mm	0.5 mm	1.0 mm
1.3 mm	1.0 mm	1.5 mm
1.6 mm	1.5 mm	2.0 mm
2.2 mm	2.0 mm	2.5 mm

In this section we can draw some conclusions as follows:

- T_ε^* values calculated from experimentally measured displacement data, quantitatively agreed with those of finite element results, in the case of 2024T3.
- The values (calculated from experimentally measured displacement s and from FEM) matched especially well, for steady state (2024T3)
- The trends (of T_ε^* calculated from experimental displacement data and from FEM) matched very well for all the cases (2024T3 and A606, various size of Γ_ε)

5. Concluding Remarks

In this paper, a method to determine the T_ε^* integral values based on given displacement data. This is the first completed research in this regard. In earlier literature [Yagawa et al. 1992)], the authors attempted to evaluate the T_ε^* integral, based on experimentally measured displacement field. In this paper, we have analyzed the nature of the T_ε^*, its physical significance and a method to evaluate it from experimentally measured displacement s. As the result of present development, one can characterize the crack tip field by evaluating the T_ε^* integral directly from experimentally measured displacements.

The methodology which was developed in this paper, can be utilized not only with moiré displacement measurement, but also with other types of techniques, such as computer image processing [see Yagawa et al. (1992)].

The findings discussed in this paper are as follows:

- T_ε^* is the measure for the rate of energy dissipated around the crack tip, for stably propagating crack in ductile materials.
- Most of contributions to the T_ε^* value is from a part of its integral contour path in front of the crack tip.
- The procedures of T_ε^* integral determination have been established. Use of deformation plasticity theory (J2-D) and "*Cut-off*" integral path are recommended.

- Comparisons between the T_ϵ^* values of finite element analysis and those evaluated from experimentally measured displacement data showed a good agreement.

The procedures of T_ϵ^* determination is utilized in Omori et al. (1995). Further discussions on the implications of T_ϵ^* are given therein.

Acknowledgments

The authors than the FAA and Mr. Chris Seher; and the Department of Energy and Dr. R. Price, for their support of this work. Also, variable discussions with Dr. F.W. Brust of Battelle Columbus Lab., Columbus OH, and Dr. L. Wang of Georgia Institute of Technology are greatly appreciated.

References

S.N. Atluri (1986): Energitic Approaches and Path Independent Integrals in Fracture Mechanics, in Computational Methods in *the Mechanics of Fracture edt. by S.N. Atluri*, North-Holland

S.N. Atluri (1997): Structural Integrity and Durability, *Tech Science Press*, Forsyth GA

S.N. Atluri, T. Nishioka and M. Nakagaki (1984): Incremental Path-Independent Integrals in Inelastic and Dynamic Fracture Mechanics, *Engineering Fracture Mechanics 20,* No.2, pp. 209-244

F.W. Brust (1984): The Use of New Path Independent Integrals in Elastic-Plastic and Creep fracture, Ph.D. Thesis, Georgia Institute of Technology

F.W. Brust, J.J. McGowan, S.N. Atluri (1986): A Combined Numerical/Experimental Study of Ductile Crack Growth After a Large Unloading, Using T*, J and CTOA Criteria, *Engineering Fracture Mechanics* 23, No. 3, pp. 537-550

F.W. Brust (1995): The T*-Integral: Definition and Use for Predicting Damage Accumulation and Fracture, in Contemporary Research in Engineering Science, edt. R.C. Batra, pp. 118-140, Springer-Verlag Berlin Heidelberg 1995

F.W. Brust, T. Nishioka and S.N. Atluri (1985): Further Studies on Elastic-Plastic Stable Fracture Utilizing The T* Integral, *Engineering Fracture Mechanics* 22, No. 6, pp. 1079-1103

J.C. Newman, D.S. Dawikie, M.A. Sutton and C.A. Bigelow (1993): A Fracture Criterion for Wide Spread Cracking in Thin Sheet Aluminum Alloys, *Int. Comittee on Aeronotical Fatigue 17th Symposium*

G.P.Nikishikov and S.N. Atluri (1987): An Equivalent Domain Integral Method for Computing Crack-Tip Integral Parameters in Non-Elastic Thermo-Mechanical Fracture, Engineering Fracture Mechanics 26, pp. 851-867

T. Nishioka, T. Fujimoto and K. Sakakura (1992): A Hybrid Numerical-Experimental Method for Caustic Measurements of the T*-Integral, , in *Fracture Mechanics 22nd Symposium ASTM STP,* 1131, pp. 170-182

H. Okada (1990): Boundary Element Methods for Linear and Nonlinear Solid Mechanics Problems: and Fracture Toughness Enhancement Mechanisms in Ceramic MaterialsPh.D.

Thesis, Georgia Institute of Technology
H. Okada and S.N. Atluri (1997): Further Studies on the Characteristics of the T_ε^* Integral: Plane Stress Stable Crack Propagation in Ductile Materials, to be published., to be published
H. Okada, T. Tamura, N. Ramakrishnan, S.N. Atluri and J.S. Epstein (1992): Analysis of Toughning of Partially Stabilized Zirconia, Due to Dilatational Transformation, Acta Metall. Mater. 40, No.6 pp 1421-1432
Y. Omori, H. Okada, S.N. Atluri and A.S. Kobayashi (1995): T* Integral Analysis for SEN Specimen using Moire Interferometry, submitted to *ATEM'95 (International Symposiu on Advanced Technology in Experimental Mechanics JSME [Japan Society of Mechanicsl Engineering])*
C.-R. Pyo, H. Okada and S.N. Atluri (1995): Regidual Strength Prediction for Aircracft Panels with Multiple Site Damage, using the "EPFEAM" for Stable Crack Growth, Computational Mechanics 16, pp. 190-196
J.R. Rice (1968): A Path Independent Integral and Approximate Analysis of Strain Concentration by Notches and Cracks, *Journal of Applied Mechanics* 35, pp. 379-386
Y. Toi and S.N. Atluri (1990a): Finite Element Analysis of Static and Dynamic Fracture of Brittle Microcracking Solids Part 1. Formulation and Simple Numerical Examples, *International Journal of Plasticity* 6, No. 2, pp. 169-188
Y. Toi and S.N. Atluri (1990b): Finite Element Analysis of Static and Dynamic Fracture of Brittle Microcracking Solids. Part 2. Stationary and Growing Macro-Cracks Under Sttic Lading, International Journal of Plasticity 6, No. 3. pp. 263-280
Y. Toi and S.N. Atluri (1990c): Finite Element Analysis of Static and Dynamic Fracture of Brittle Microcracking Solids. Part 3. Stationary and Rapidly Propagation Cracks Under Dynamic Loading, *International Journal of Plasticity* 6, No. 4, pp. 389-414
L. Wang, F.W. Brust and S.N. Atluri (1995a): Elastic-Plastic Finite Element Alternating Method and Prediction of Fracture, Part 1: EPFEAM theory
L. Wang, F.W. Brust and S.N. Atluri (1995b): Elastic-Plastic Finite Element Alternating Method and Prediction of Fracture, Part 2: Fracture T* Integral Parameter
L. Wang, F.W. Brust and S.N. Atluri (1995c): Elastic-Plastic Finite Element Alternating Method and Prediction of Fracture, Part 3: Application Prediction of the NIST Multiple Site Damage Experiments
J.R. Willis (1975): Equations of Motion for Propagating Cracks, *in the Mechanics ands Physiscs of Fracture*, Metals Society/Institute of Physics
G. Yagawa, S. Yoshimura, A. Yoshioka and C.-R. Pyo (1992): Analysis of Growing Ductile Cracks Using Computer Image Processing, in *Fracture Mechanics 22nd Symposium ASTM STP*, 1131, pp. 289-313

List of Figures

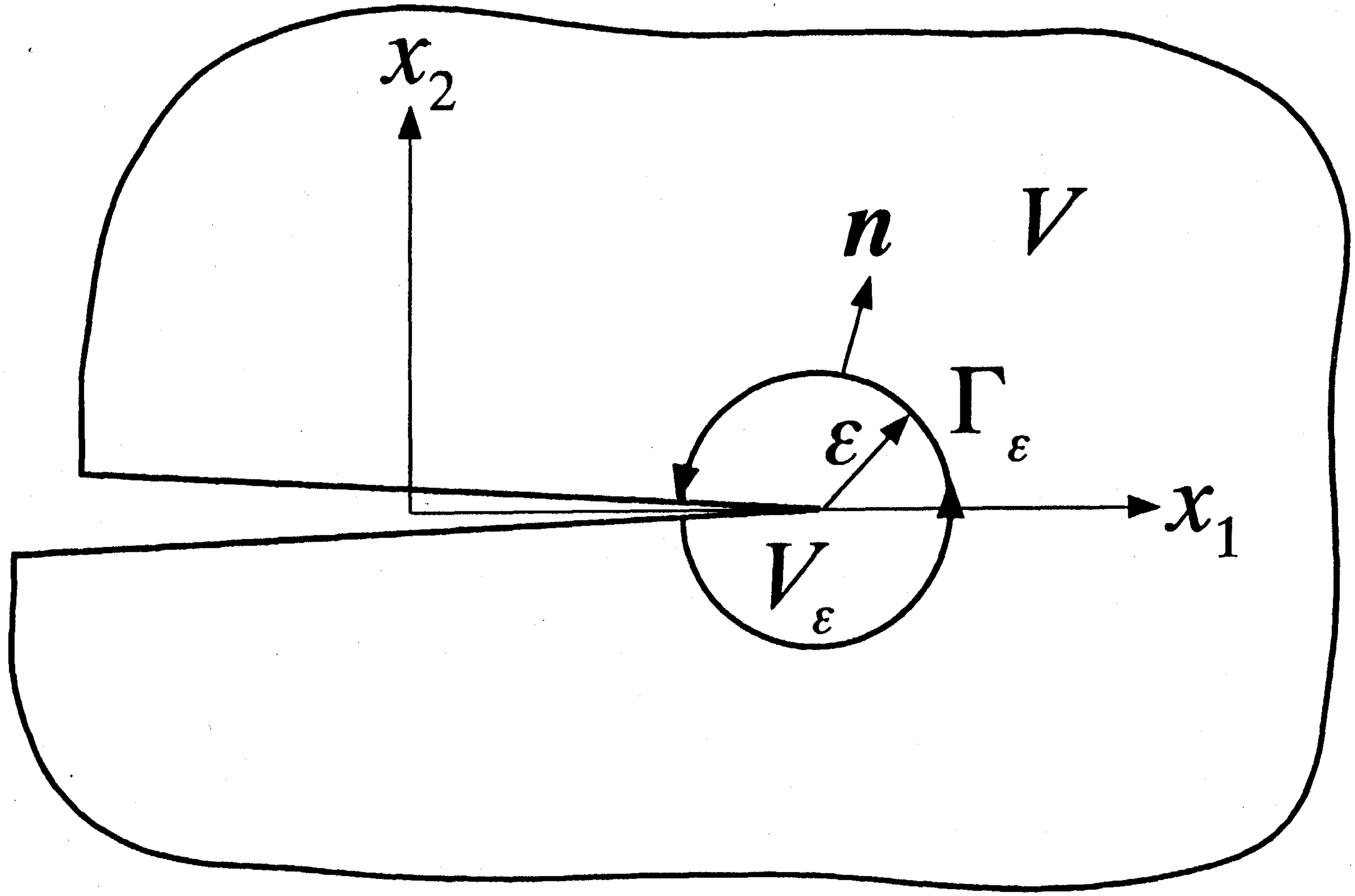

Fi

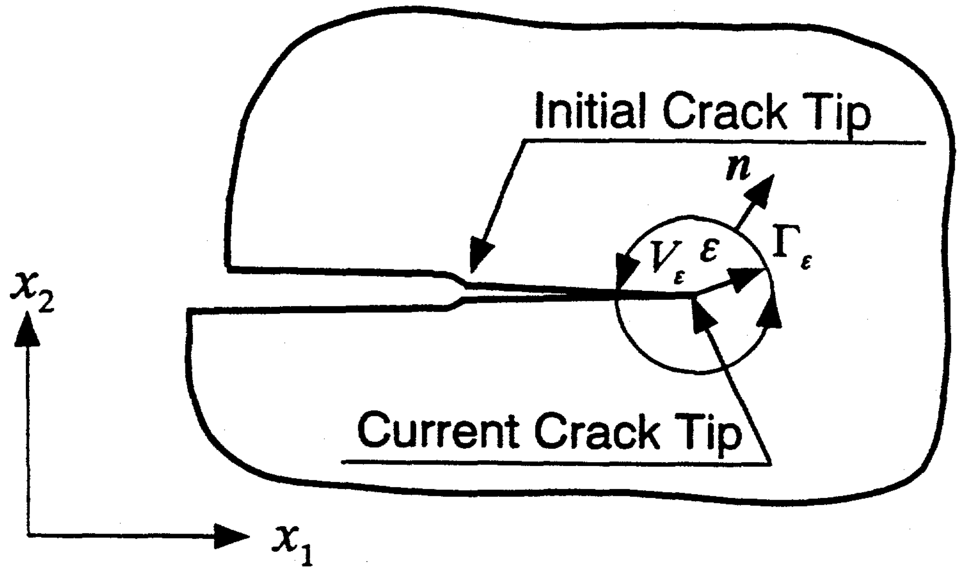

(a) Moving Contour

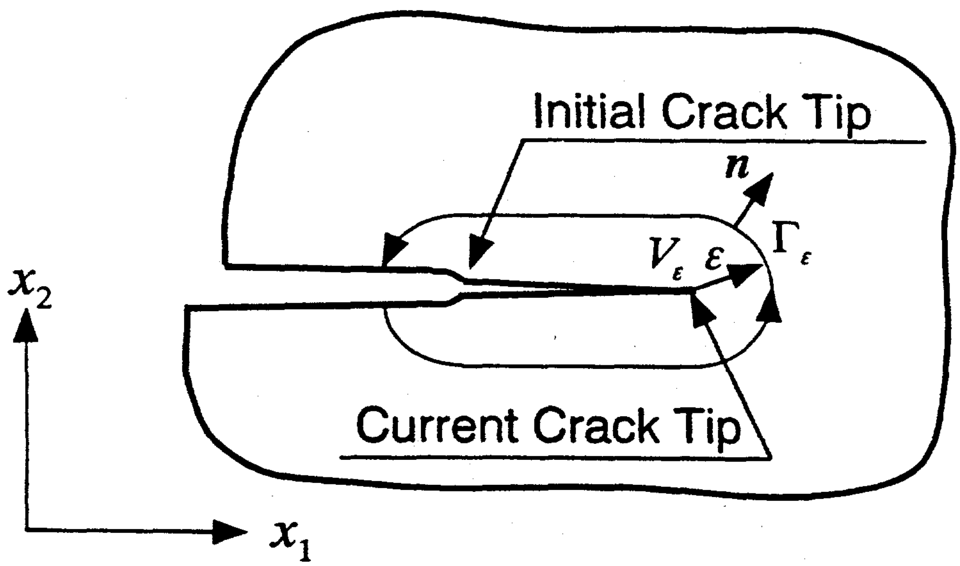

(b) Elongating Contour

Figure 2 (a) and (b)

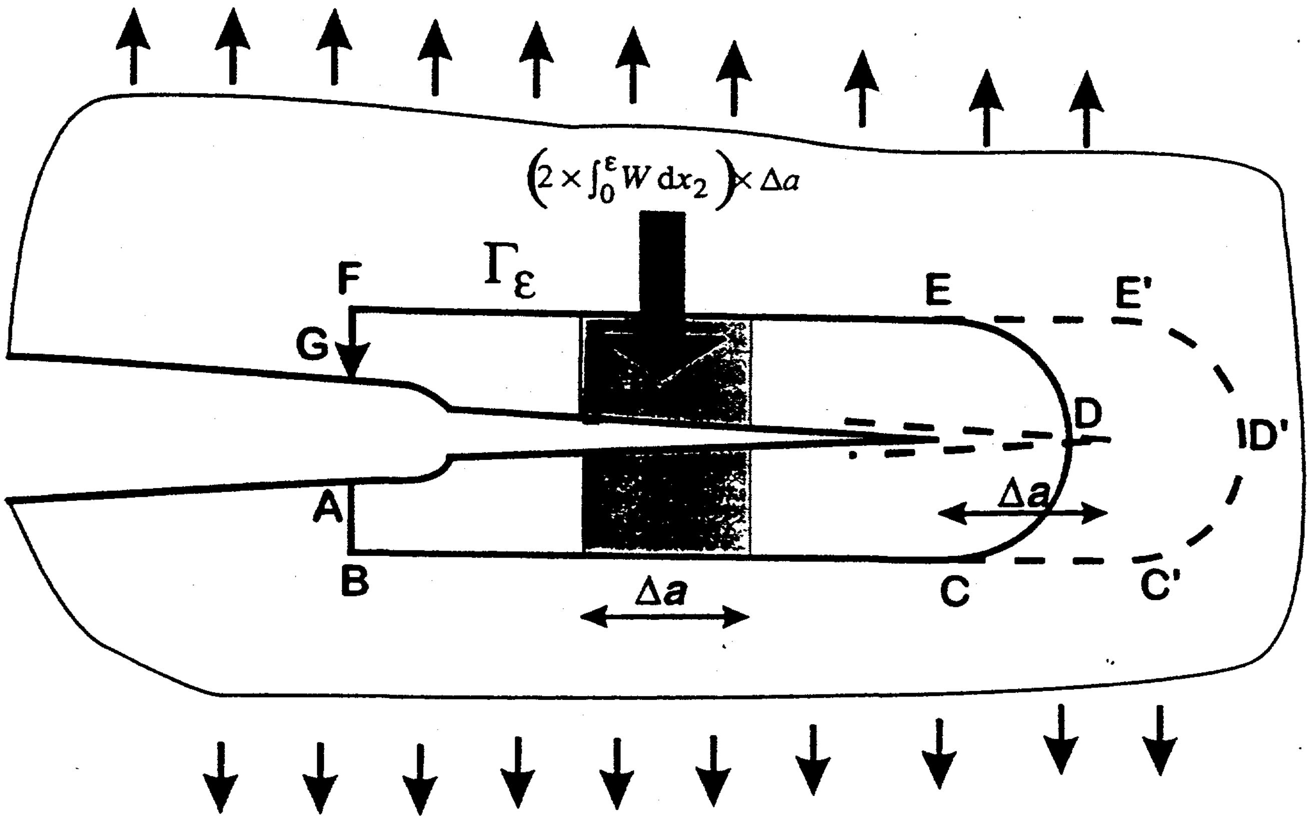
$\left(2\times\int_0^\varepsilon W\,dx_2\right)\times\Delta a$
Γ_ε
F
G
E
E'
D
D'
A
B
C
C'
Δa
Δa

Figure 3.

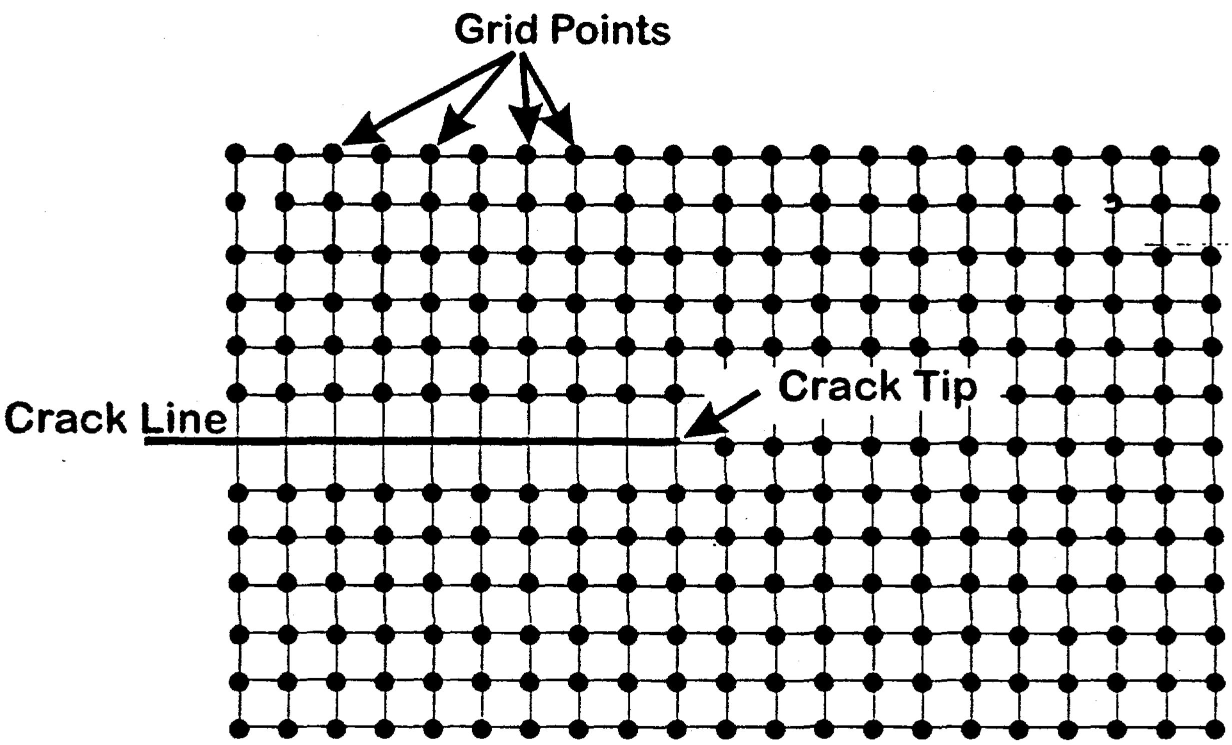

Figure 4

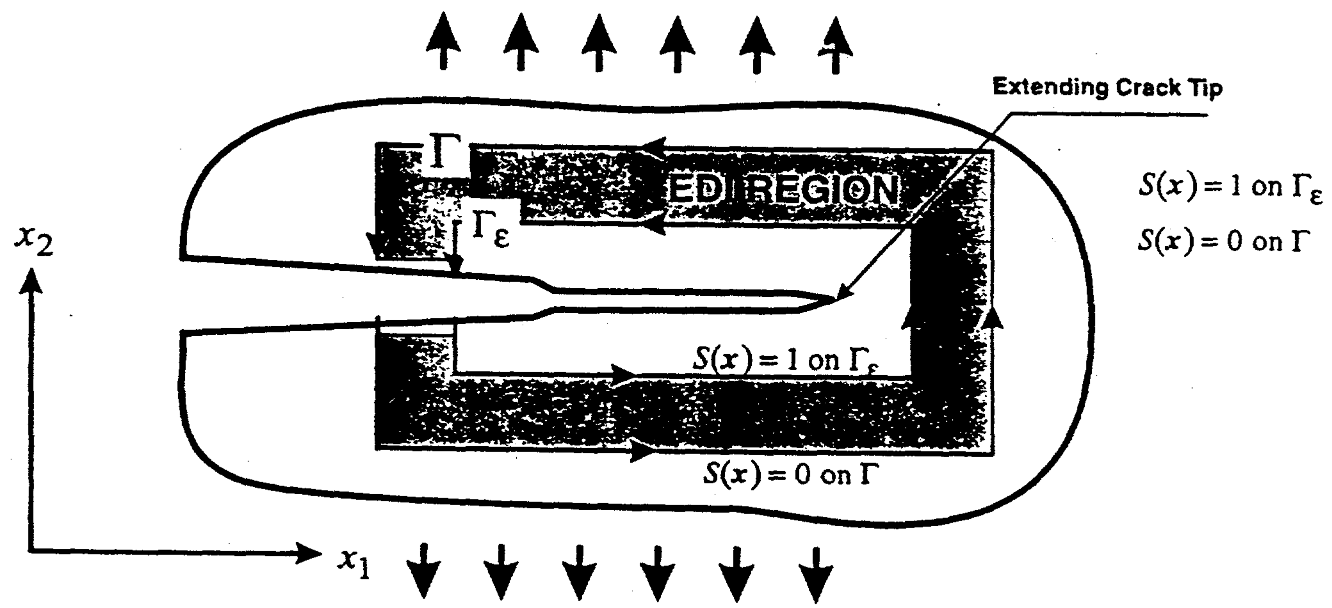

$$T_{\varepsilon}^{*} = \int_{\Gamma_{\varepsilon}} \left(W n_1^{\varepsilon} - n_i^{\varepsilon} \sigma_{ij} \frac{\partial u_j}{\partial x_1} \right) d\Gamma_{\varepsilon} = -\int_{A-A_{\varepsilon}} \left(\frac{\partial [S(x) W]}{\partial x_1} - \frac{\partial \left[S(x) \sigma_{ij} \frac{\partial u_j}{\partial x_1} \right]}{\partial x_i} \right) d(A - A_{\varepsilon})$$

Figure 5

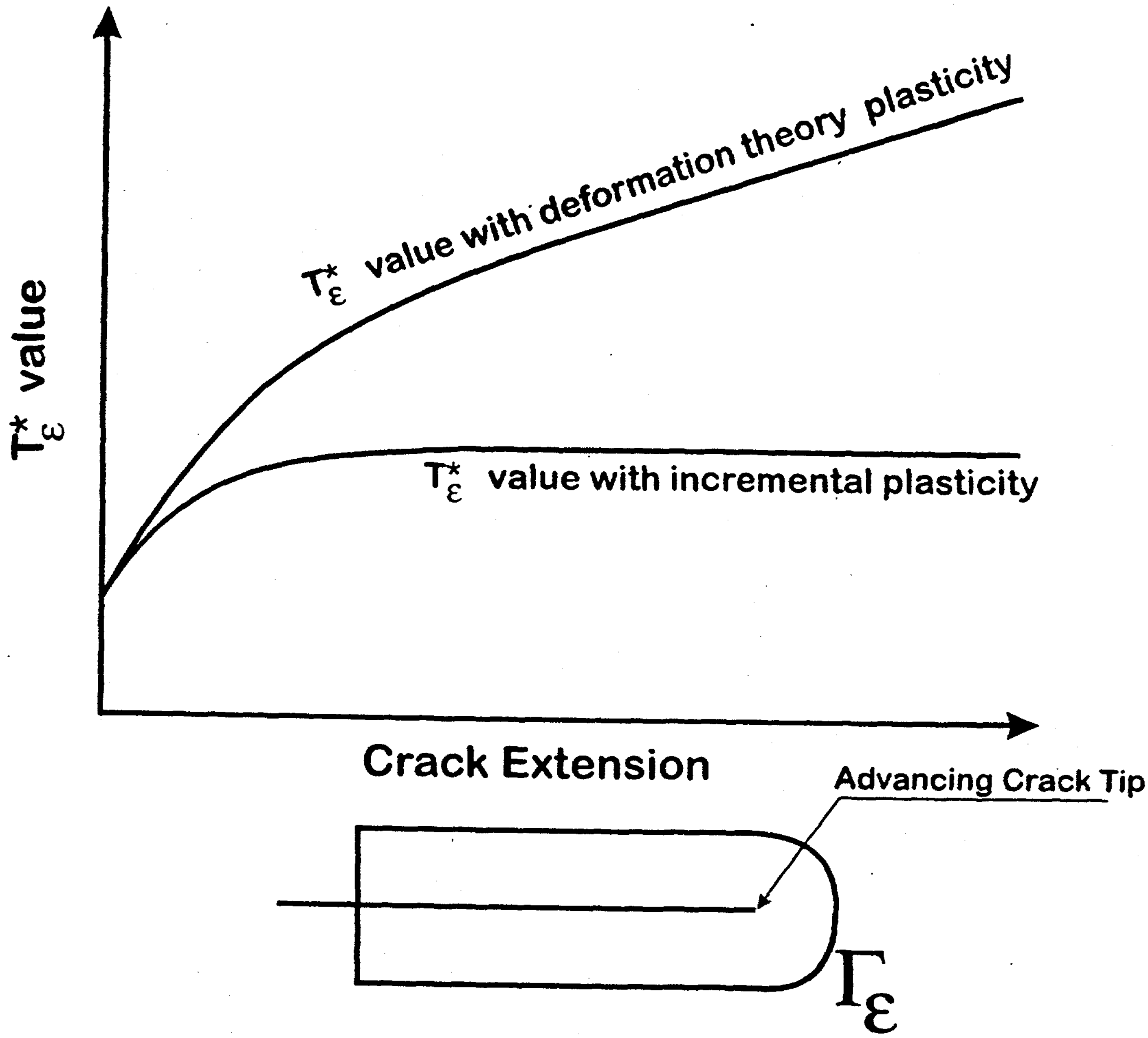
T^*_ε value with deformation theory plasticity
T^*_ε value with incremental plasticity
T^*_ε value
Crack Extension
Advancing Crack Tip
Γ_ε

Figure 6

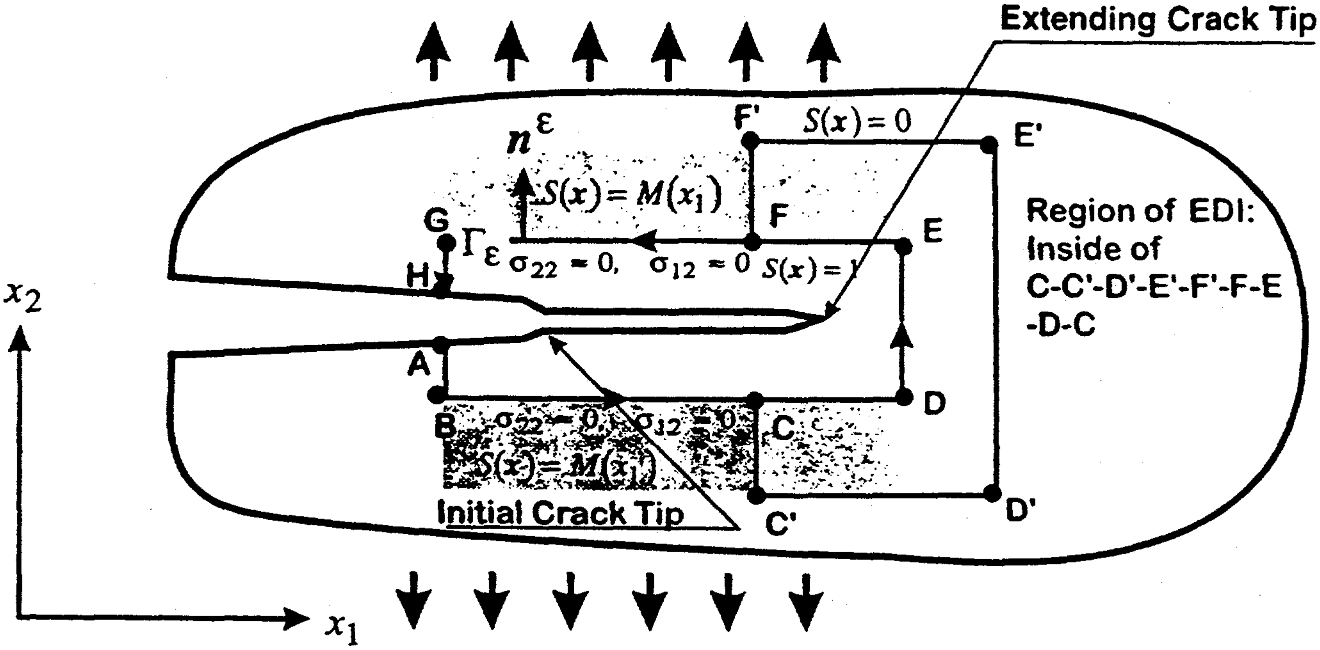

$S(x)=1$: on A-B-C-D-E-F-G-H

$S(x)=0$: on C'-D'-E'F'

$S(x)=M(x_1)$: in Shaded Regions

(a)

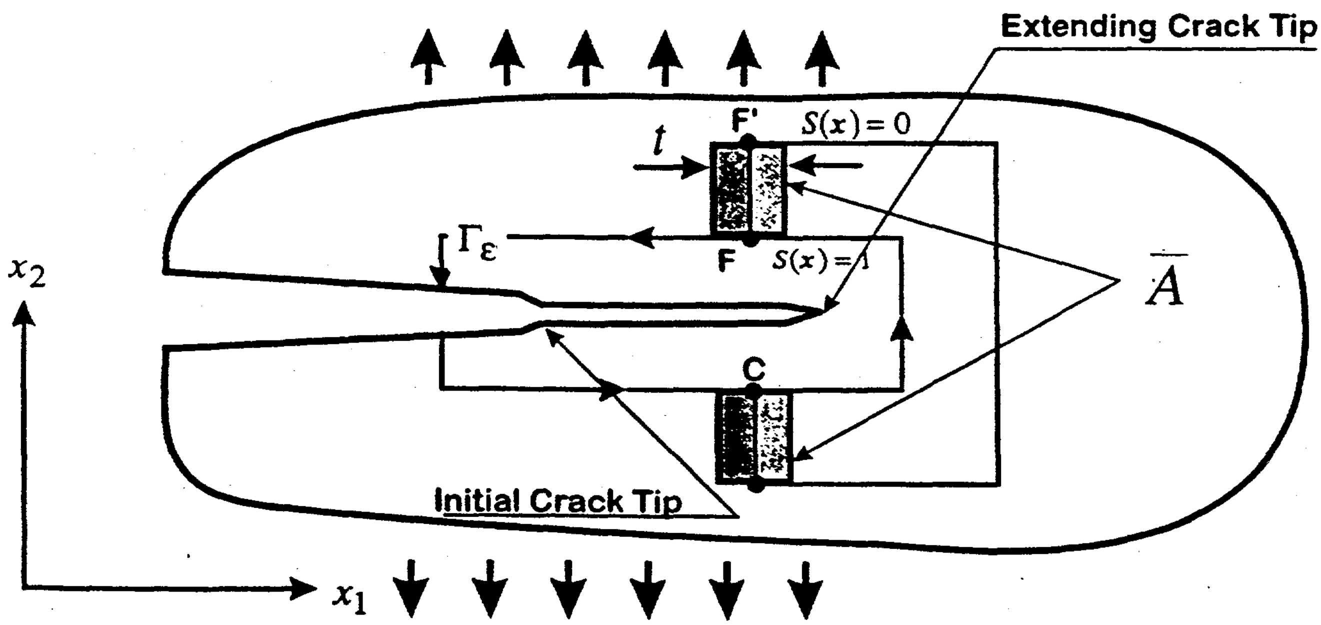

$S(x)=M(x_1)$: in $\bar{A}$

(b)

Figure 7

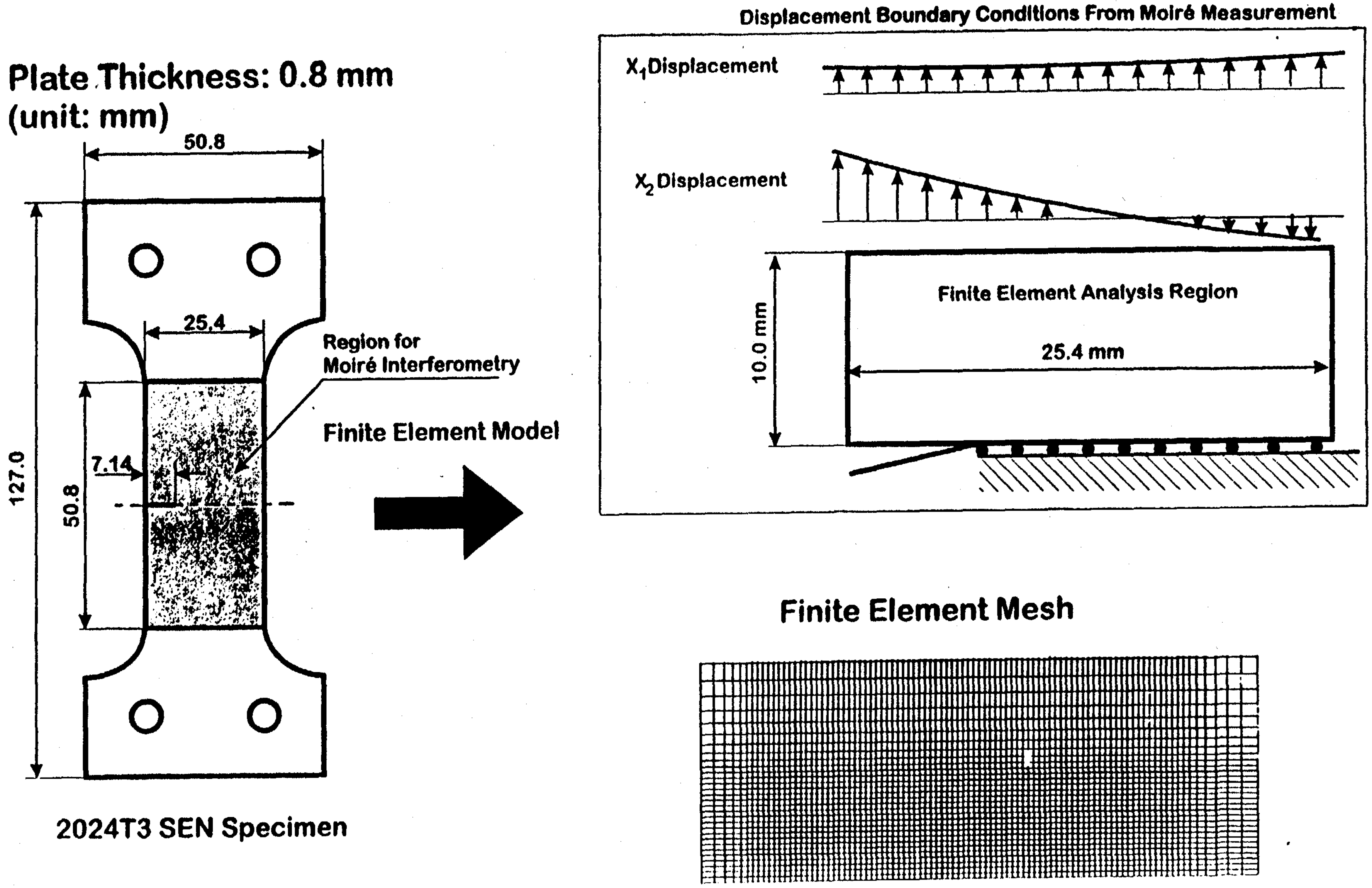
Plate Thickness: 0.8 mm
(unit: mm)
50.8
25.4
127.0
50.8
7.14
Region for
Moiré Interferometry
Finite Element Model
2024T3 SEN Specimen
Displacement Boundary Conditions From Moiré Measurement
X1 Displacement
X2 Displacement
10.0 mm
Finite Element Analysis Region
25.4 mm
Finite Element Mesh

Figure 8

MATERIAL PROPERTIES OF 2024T3

Young's Modulus: 75 GPa
Poison's Ratio: 0.33
Plate Thickness: 0.8 mm

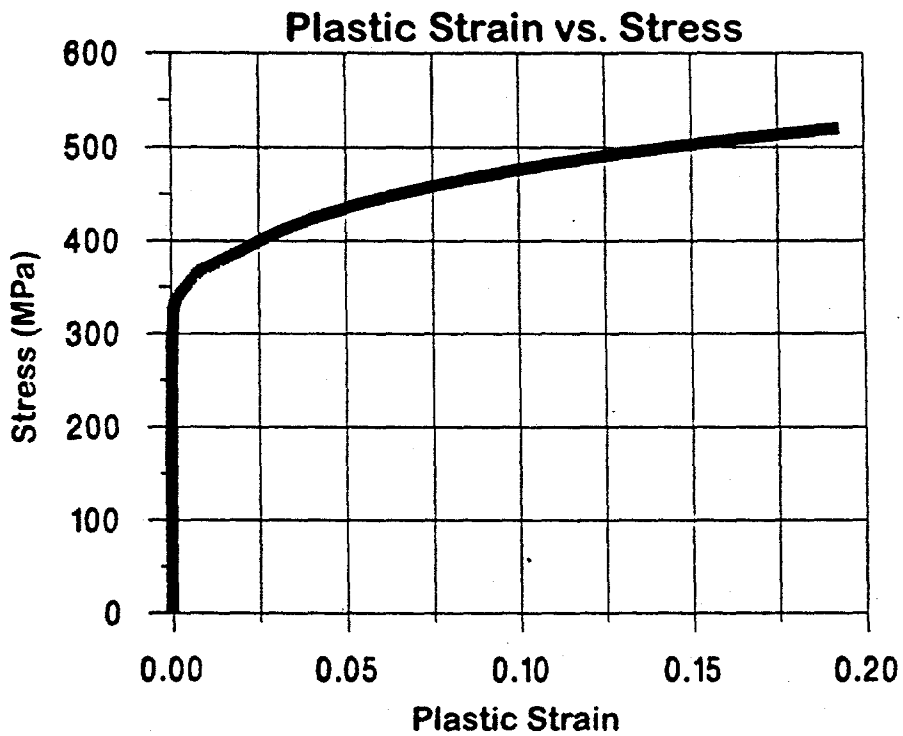

Figure 9

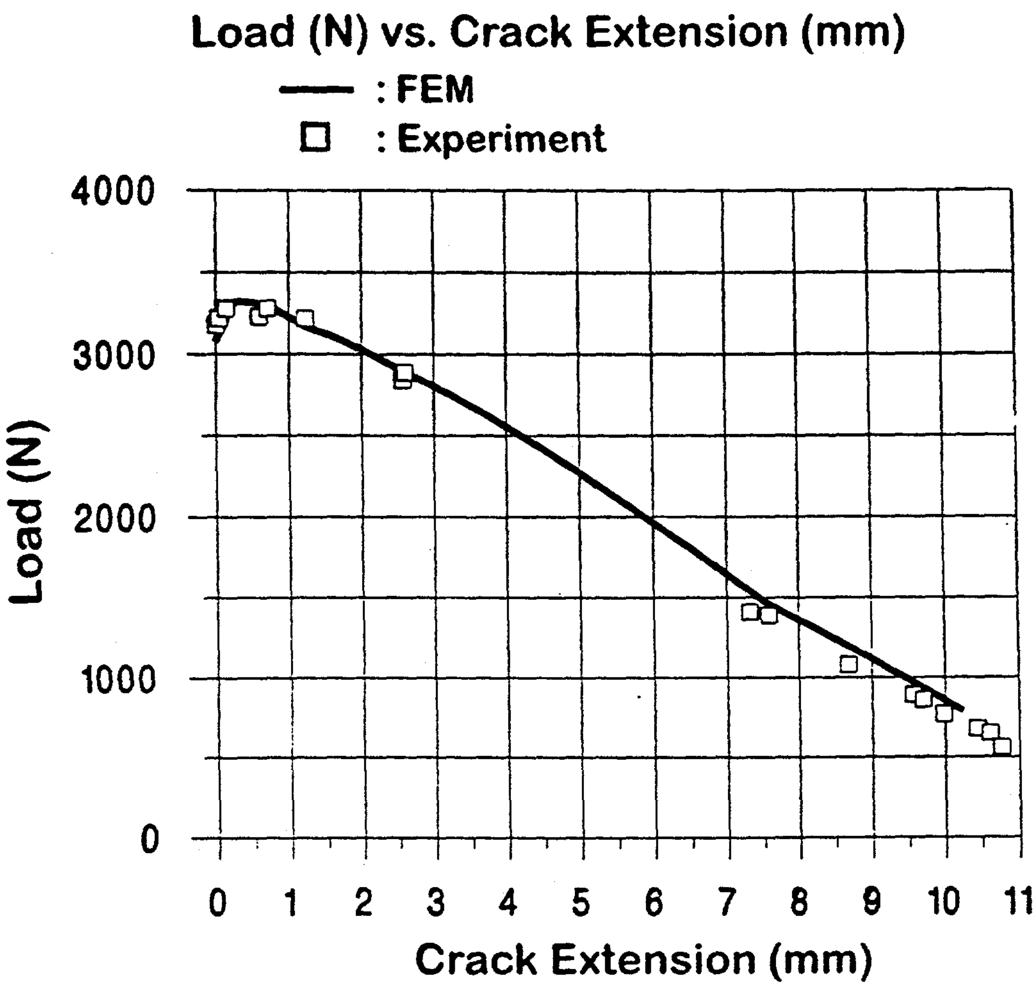

Load (N) vs. Crack Extension (mm)
: FEM
: Experiment
4000
3000
2000
1000
0
Load (N)
0
1
2
3
4
5
6
7
8
9
10
11
Crack Extension (mm)

Figure 10

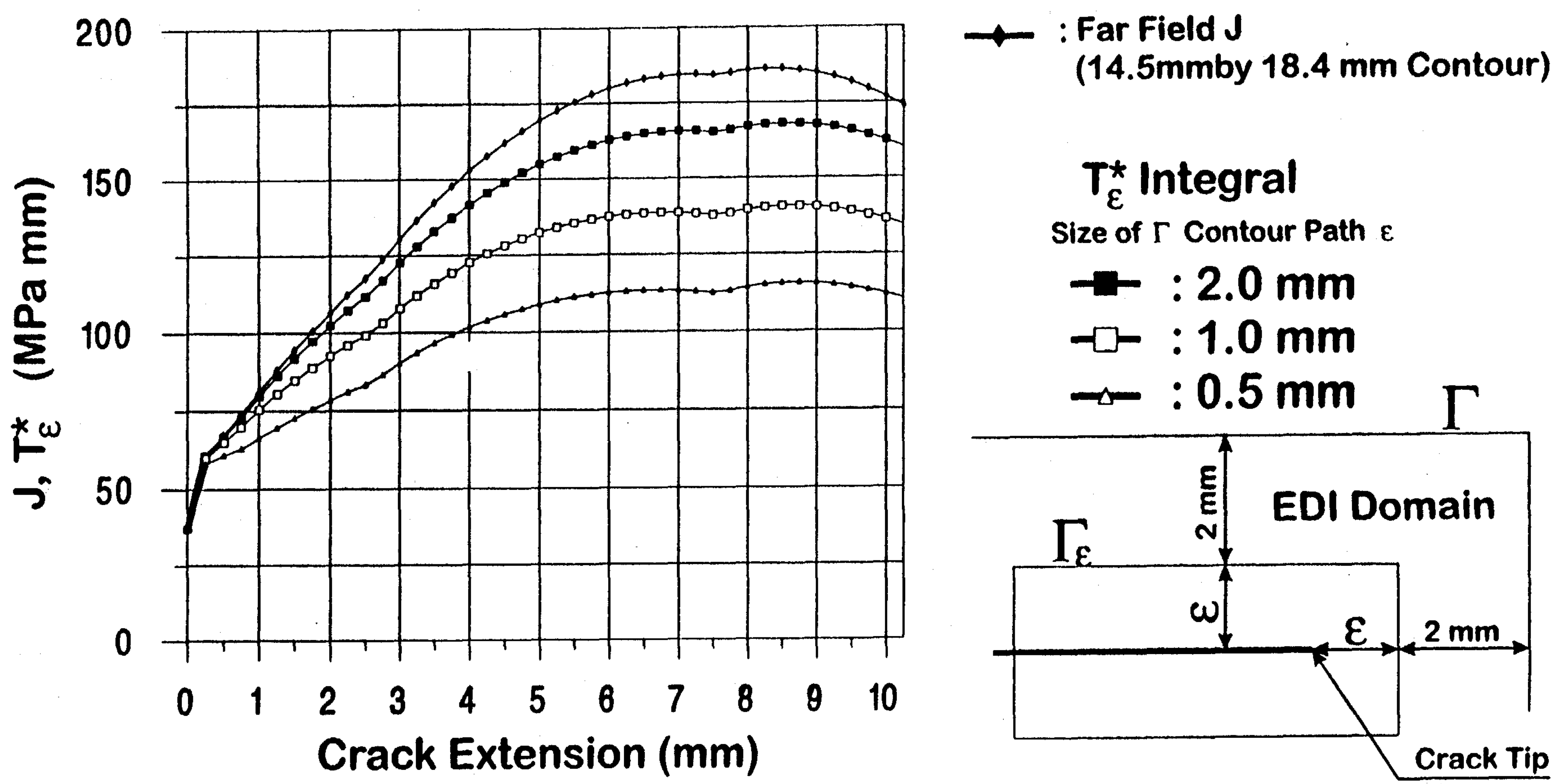

: Far Field J
(14.5mmby 18.4 mm Contour)
T^*_ε Integral
Size of Γ Contour Path ε
: 2.0 mm
: 1.0 mm
: 0.5 mm
200
150
100
50
0
J, T^*_ε (MPa mm)
0
1
2
3
4
5
6
7
8
9
10
Crack Extension (mm)
Γ
Γ_ε
2 mm
EDI Domain
ε
ε
2 mm
Crack Tip

Figure 11

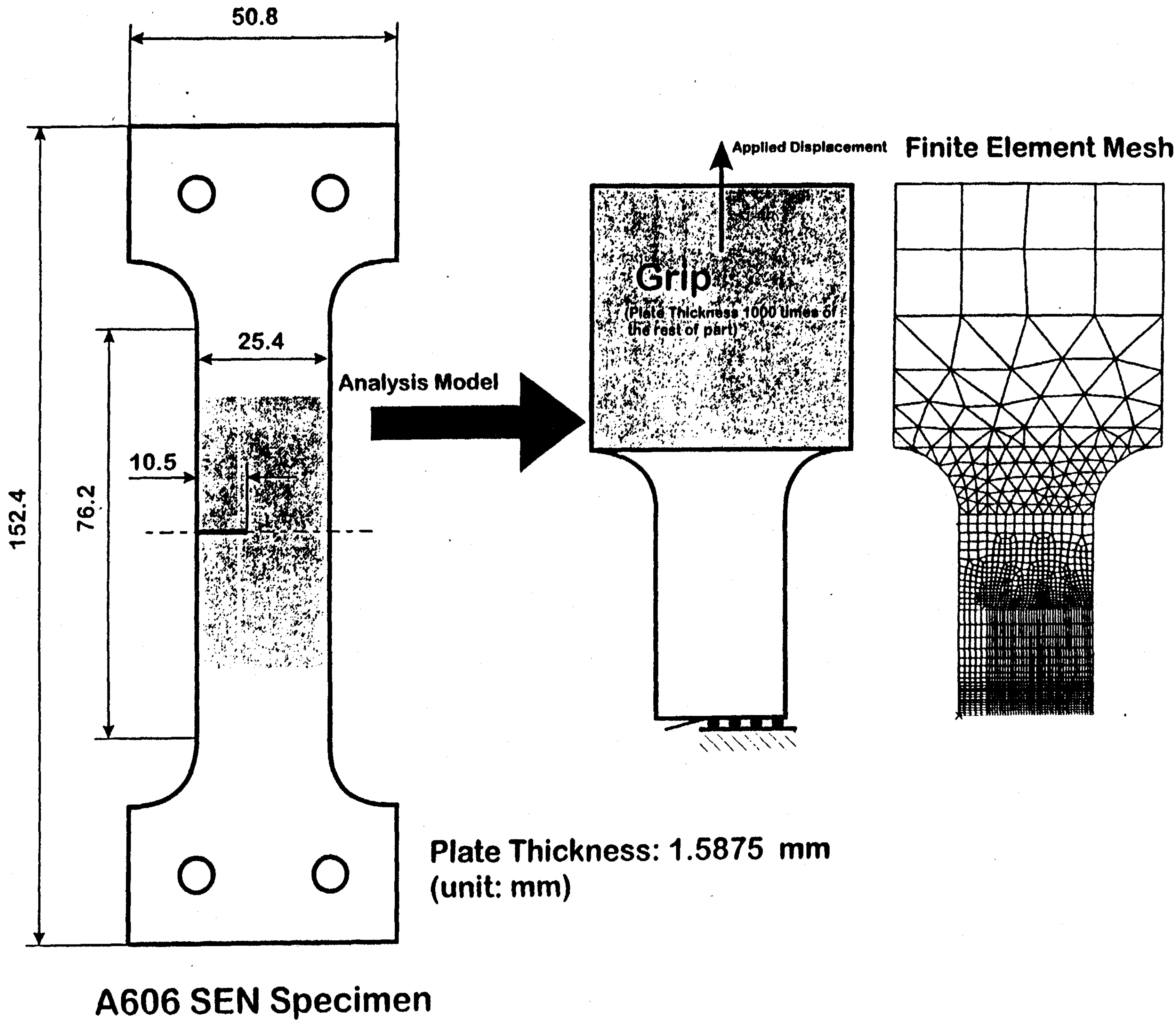
50.8
152.4
76.2
25.4
10.5
Analysis Model
Applied Displacement
Grip
(Plate Thickness 1000 times of the rest of part)
Finite Element Mesh
Plate Thickness: 1.5875 mm
(unit: mm)
A606 SEN Specimen

Figure 12

Material Properties of A606

Young's Modulus: 202400.3 MPa
Poison's Ratio: 2.950E-01
Plate Thickness: 1.5875 mm

Stress-Plastic Strain Curve

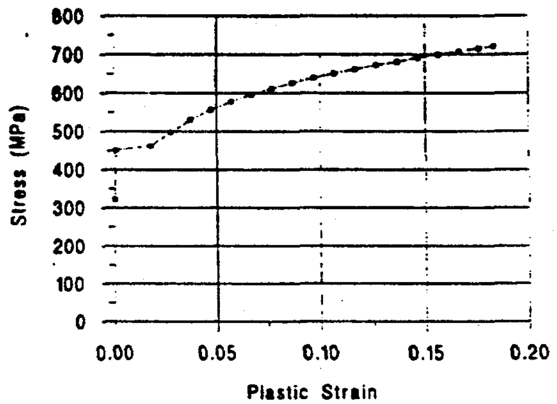

Figure 13

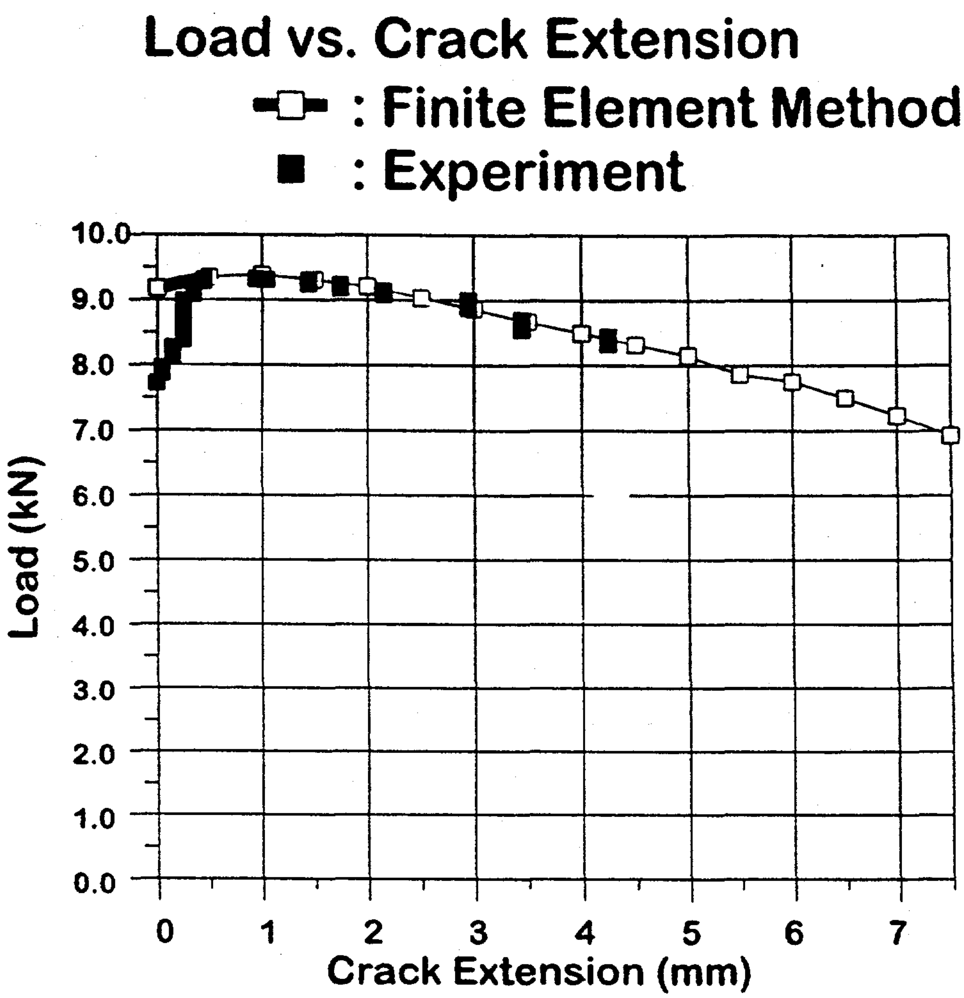

Load vs. Crack Extension
: Finite Element Method
: Experiment
10.0
9.0
8.0
7.0
6.0
5.0
4.0
3.0
2.0
1.0
0.0
Load (kN)
0
1
2
3
4
5
6
7
Crack Extension (mm)

Figure 14

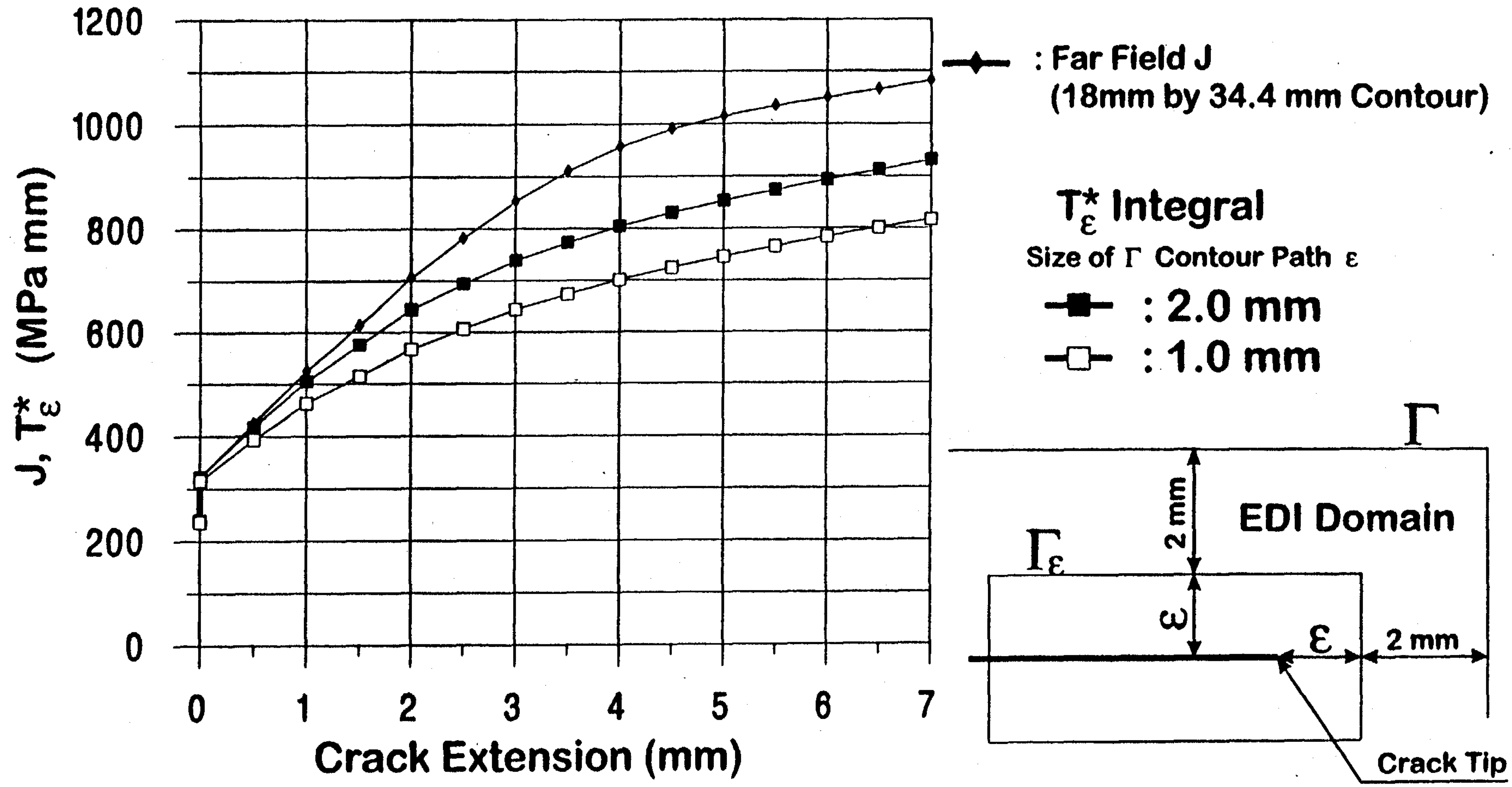

1200
1000
800
600
400
200
0
J, T^*_ε (MPa mm)
0
1
2
3
4
5
6
7
Crack Extension (mm)
: Far Field J
(18mm by 34.4 mm Contour)
T^*_ε Integral
Size of Γ Contour Path ε
: 2.0 mm
: 1.0 mm
Γ
Γε
EDI Domain
2 mm
ε
ε
2 mm
Crack Tip

Figure 15

Plastic Zone at Crack Propagation Initiation

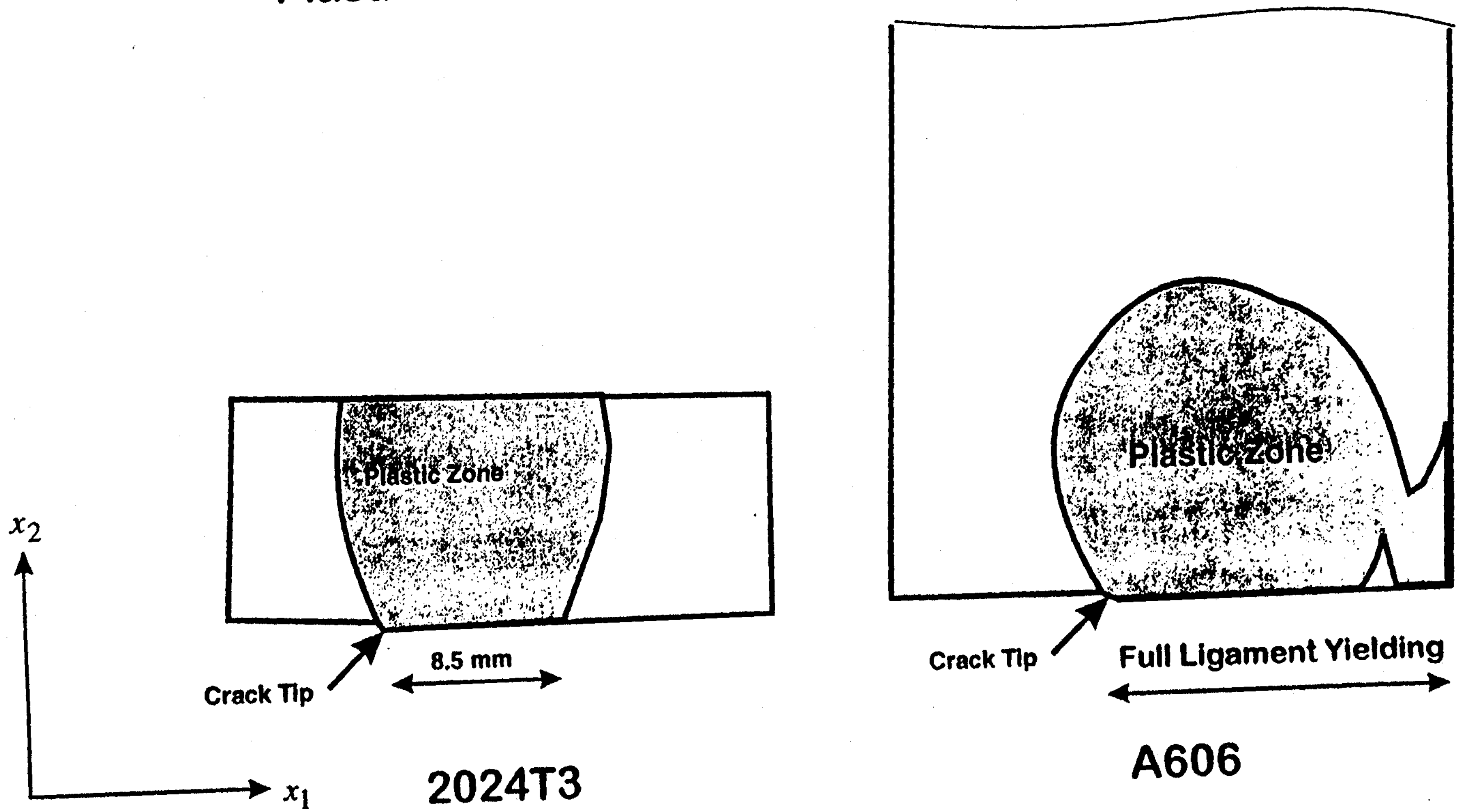

Figure 16

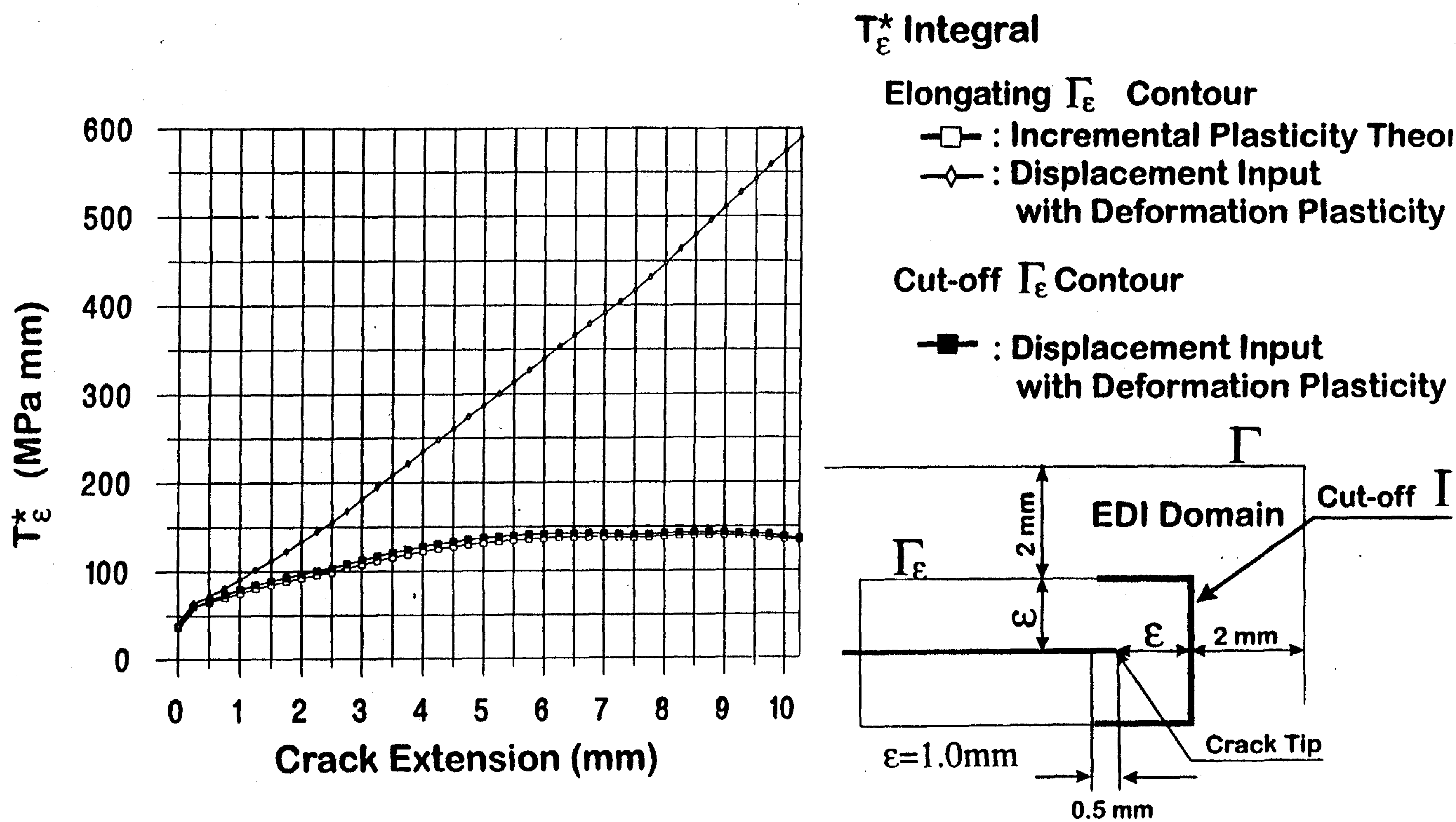

T^*_ε (MPa mm)
600
500
400
300
200
100
0
0
1
2
3
4
5
6
7
8
9
10
Crack Extension (mm)
T^*_ε Integral
Elongating Γ_ε Contour
: Incremental Plasticity Theo
: Displacement Input with Deformation Plasticity
Cut-off Γ_ε Contour
: Displacement Input with Deformation Plasticity
Γ
EDI Domain
Cut-off Γ
2 mm
Γ_ε
ε
ε
2 mm
Crack Tip
ε=1.0mm
0.5 mm

Figure 17

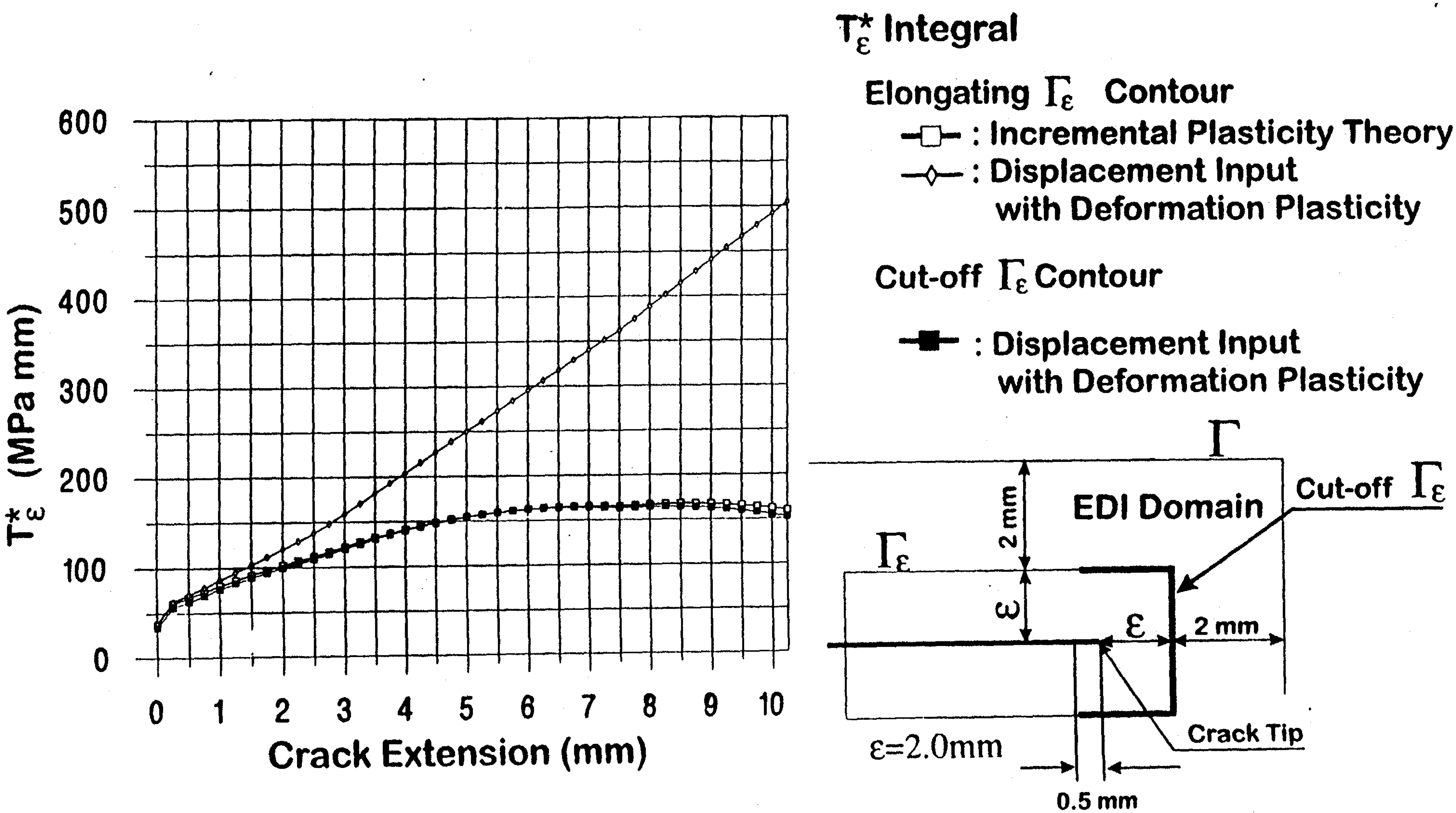

T*ε Integral
Elongating Γε Contour
: Incremental Plasticity Theory
: Displacement Input with Deformation Plasticity
Cut-off Γε Contour
: Displacement Input with Deformation Plasticity
600
500
400
300
200
100
0
T*ε (MPa mm)
0 1 2 3 4 5 6 7 8 9 10
Crack Extension (mm)
Γ
EDI Domain
Cut-off Γε
Γε
2 mm
ε
ε
2 mm
Crack Tip
ε=2.0mm
0.5 mm

Figure 18

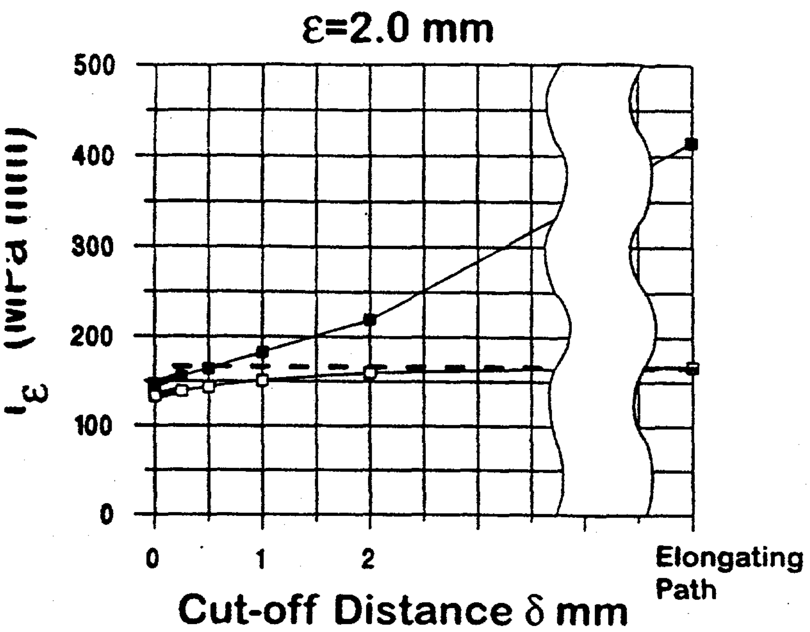

(a) ε=2.0 mm

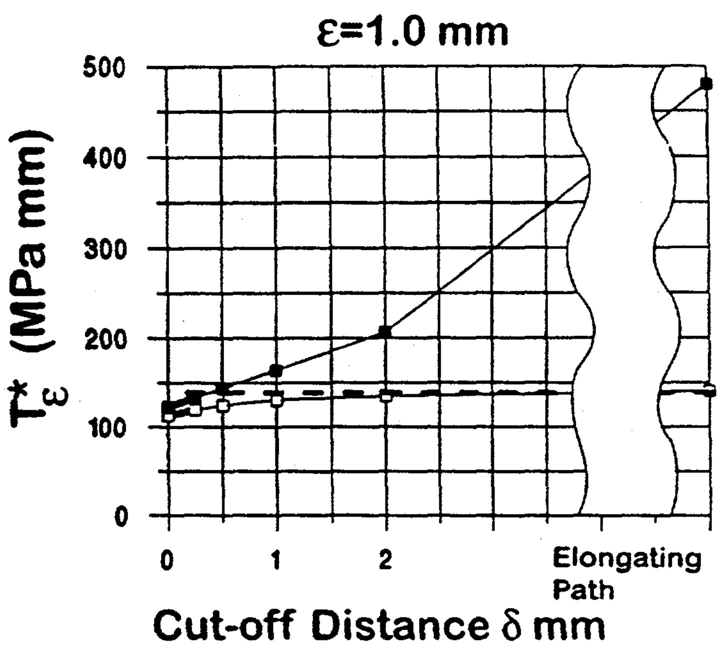

(b) ε=1.0 mm

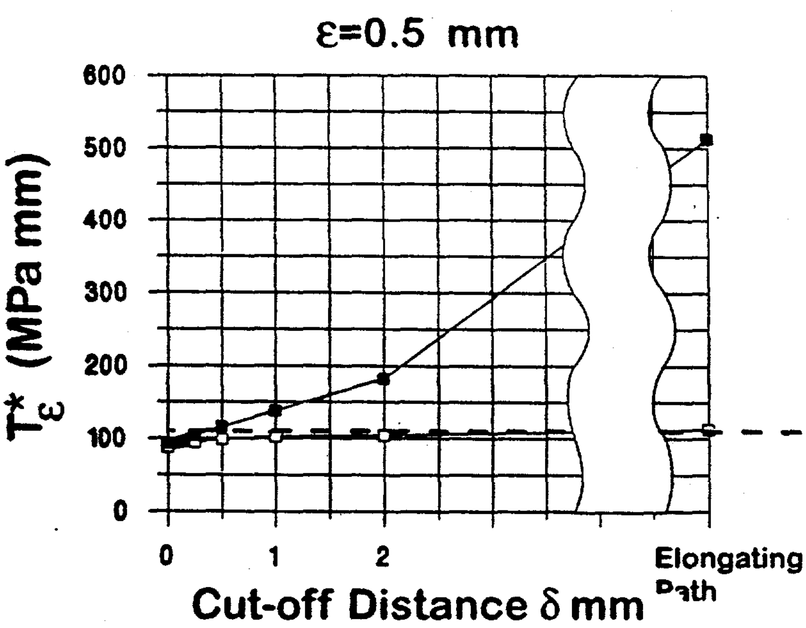

(c) ε=0.5 mm

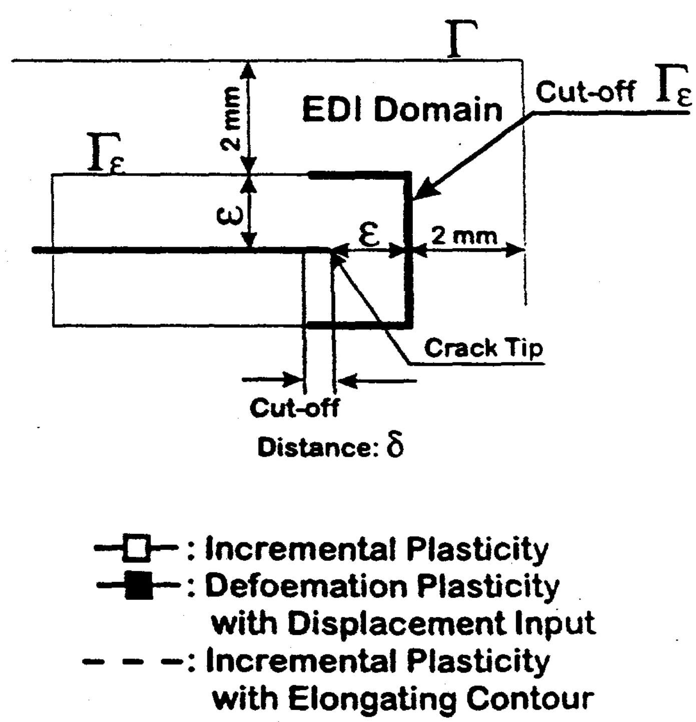

Figure 19

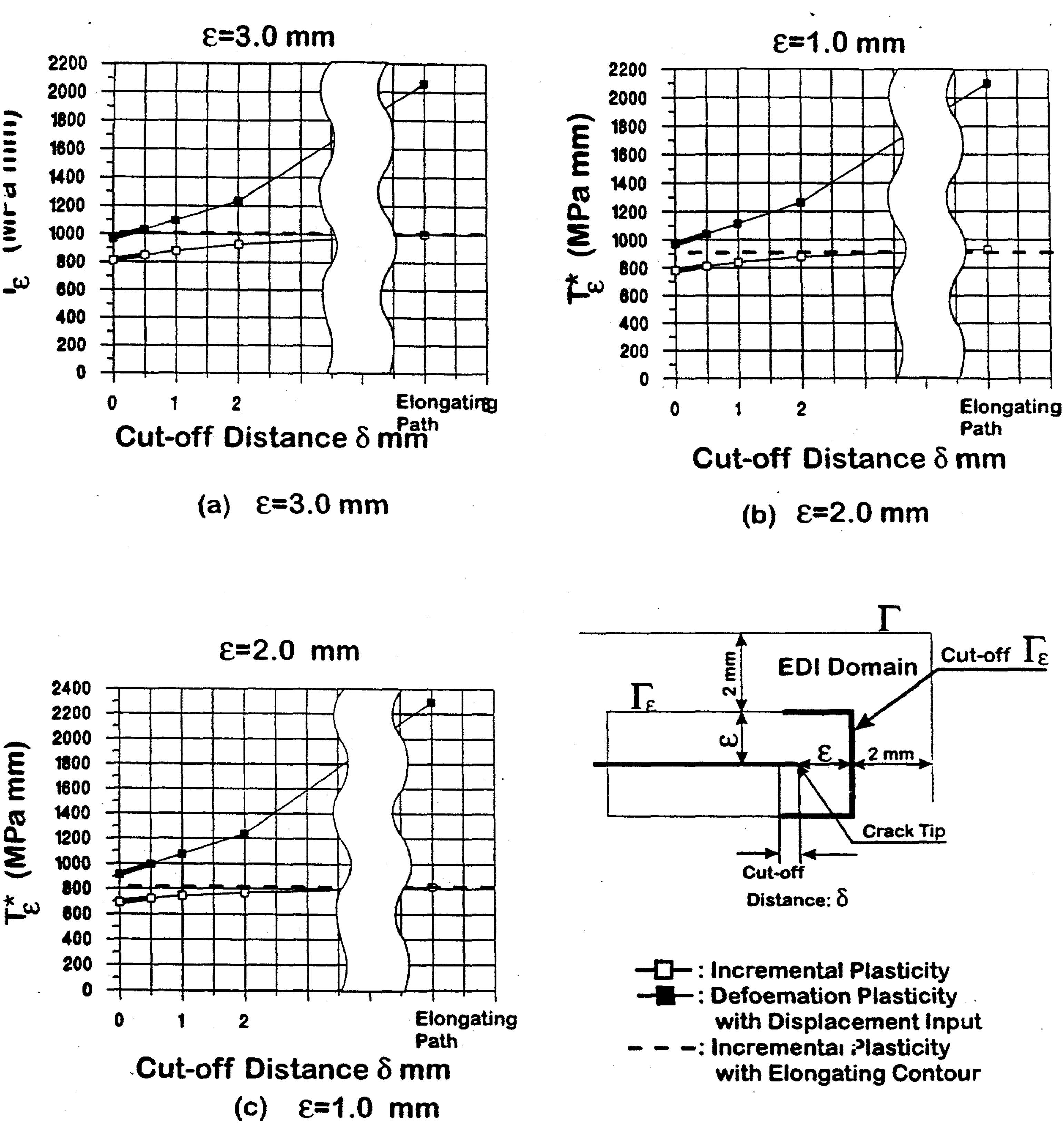
ε=3.0 mm
2200
2000
1800
1600
1400
1200
1000
800
600
400
200
0
0
1
2
Elongating Path
Cut-off Distance δ mm
(a) ε=3.0 mm
ε=1.0 mm
T*ε (MPa mm)
Elongating Path
Cut-off Distance δ mm
(b) ε=2.0 mm
ε=2.0 mm
2400
T*ε (MPa mm)
Elongating Path
Cut-off Distance δ mm
(c) ε=1.0 mm
Γ
EDI Domain
Cut-off Γε
Γε
2 mm
ε
ε
2 mm
Crack Tip
Cut-off
Distance: δ
: Incremental Plasticity
: Defoemation Plasticity
with Displacement Input
: Incrementai ?lasticity
with Elongating Contour

Figure 20

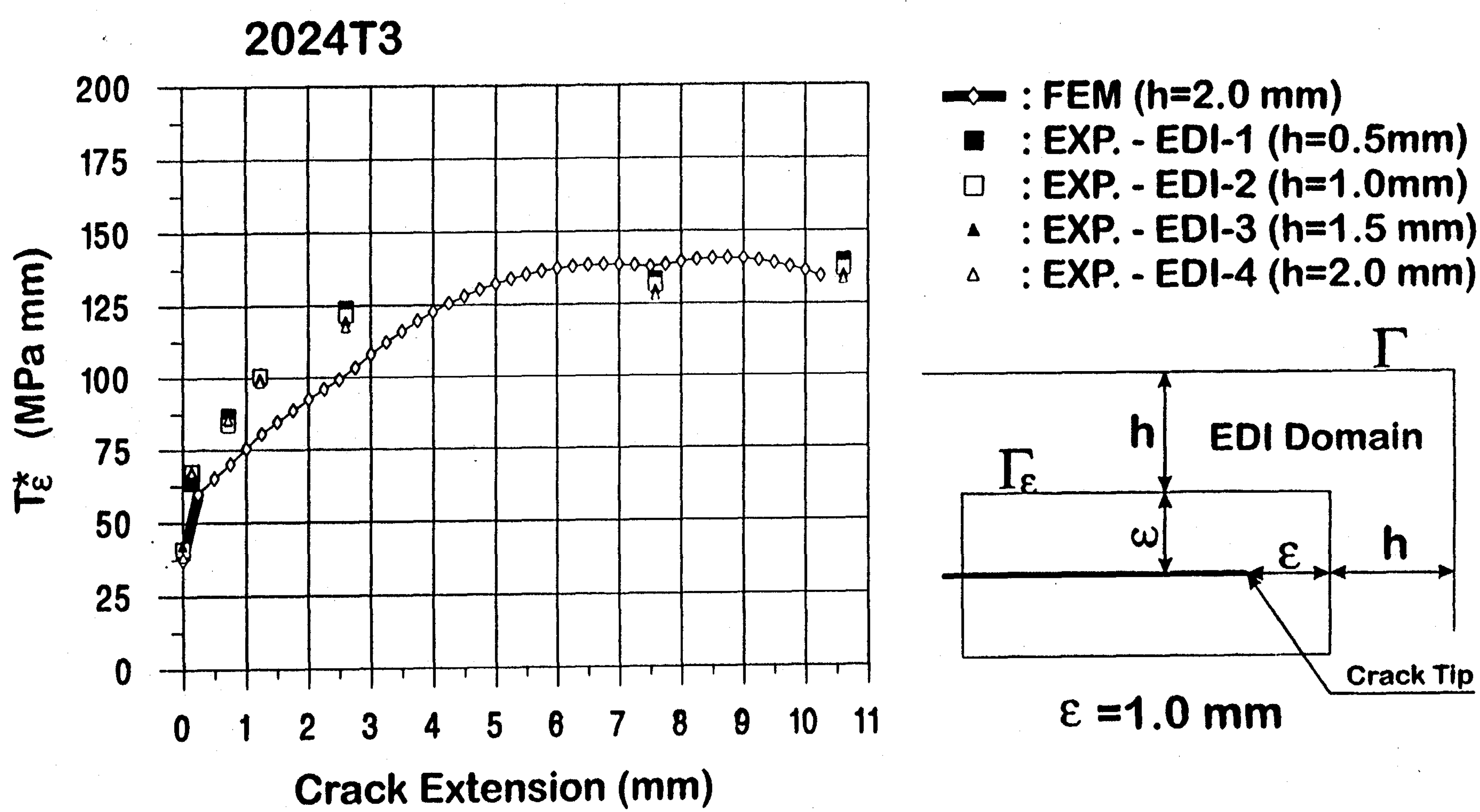
2024T3
T^*_ε (MPa mm)
200
175
150
125
100
75
50
25
0
0
1
2
3
4
5
6
7
8
9
10
11
Crack Extension (mm)
: FEM (h=2.0 mm)
: EXP. - EDI-1 (h=0.5mm)
: EXP. - EDI-2 (h=1.0mm)
: EXP. - EDI-3 (h=1.5 mm)
: EXP. - EDI-4 (h=2.0 mm)
Γ
h
EDI Domain
Γ_ε
ω
ε
h
Crack Tip
ε =1.0 mm

Figure 21

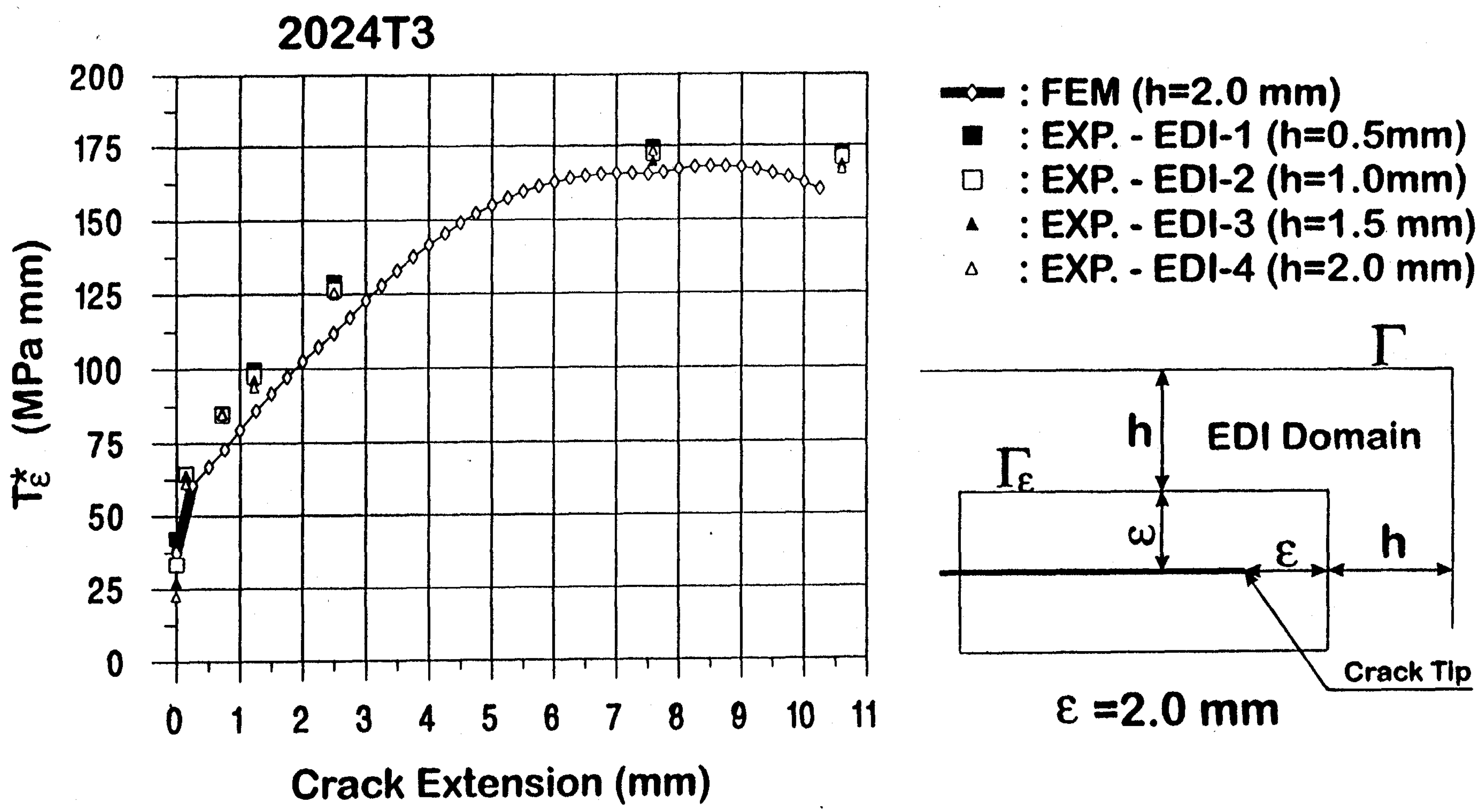
2024T3
200
175
150
125
100
75
50
25
0
T^*_ε (MPa mm)
0
1
2
3
4
5
6
7
8
9
10
11
Crack Extension (mm)
: FEM (h=2.0 mm)
: EXP. - EDI-1 (h=0.5mm)
: EXP. - EDI-2 (h=1.0mm)
: EXP. - EDI-3 (h=1.5 mm)
: EXP. - EDI-4 (h=2.0 mm)
Γ
h
EDI Domain
Γ_ε
ω
ε
h
Crack Tip
ε =2.0 mm

Figure 22

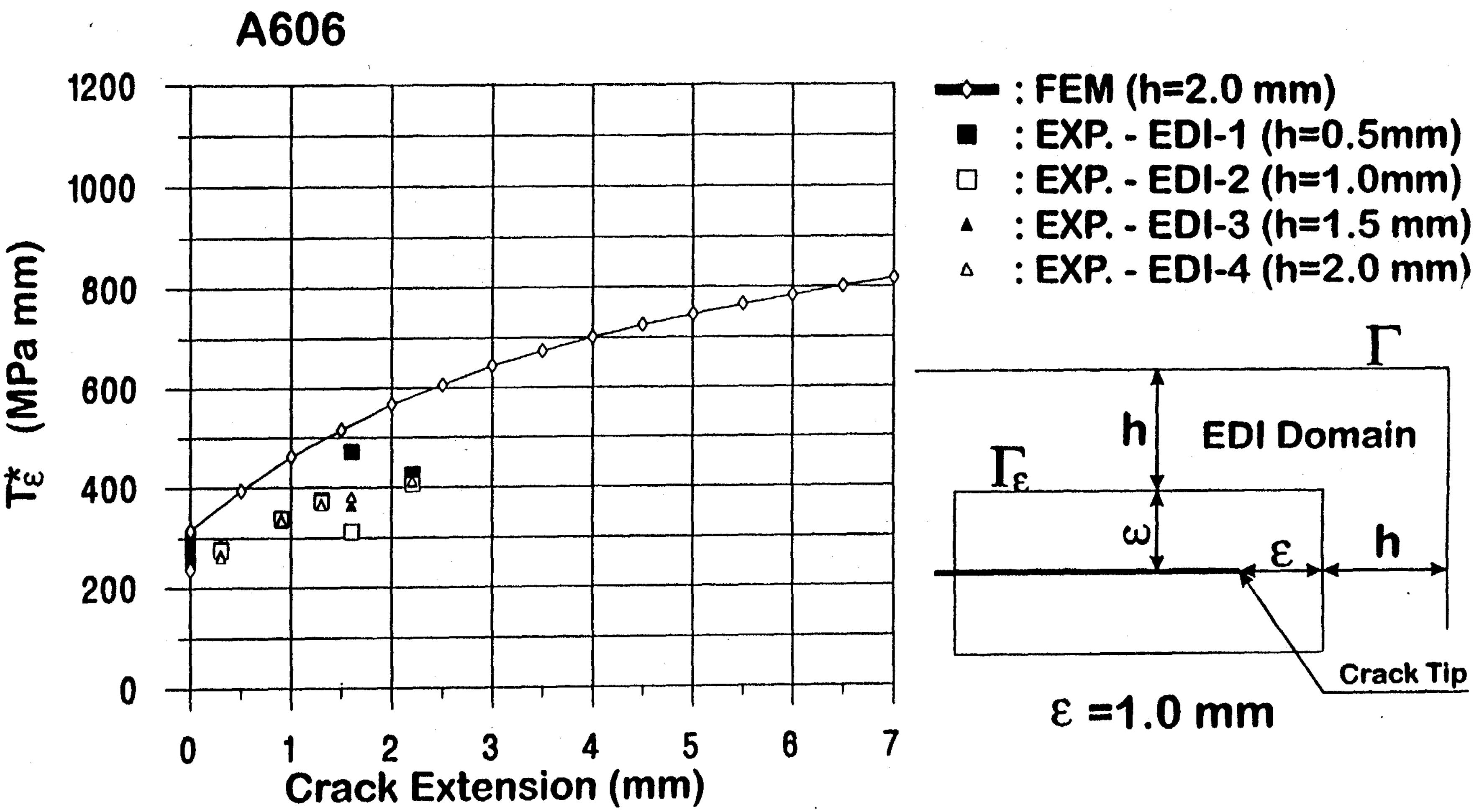
A606
1200
1000
800
600
400
200
0
T^*_ε (MPa mm)
0
1
2
3
4
5
6
7
Crack Extension (mm)
: FEM (h=2.0 mm)
: EXP. - EDI-1 (h=0.5mm)
: EXP. - EDI-2 (h=1.0mm)
: EXP. - EDI-3 (h=1.5 mm)
: EXP. - EDI-4 (h=2.0 mm)
Γ
h
EDI Domain
Γ_ε
ω
ε
h
Crack Tip
ε =1.0 mm

Figure 23

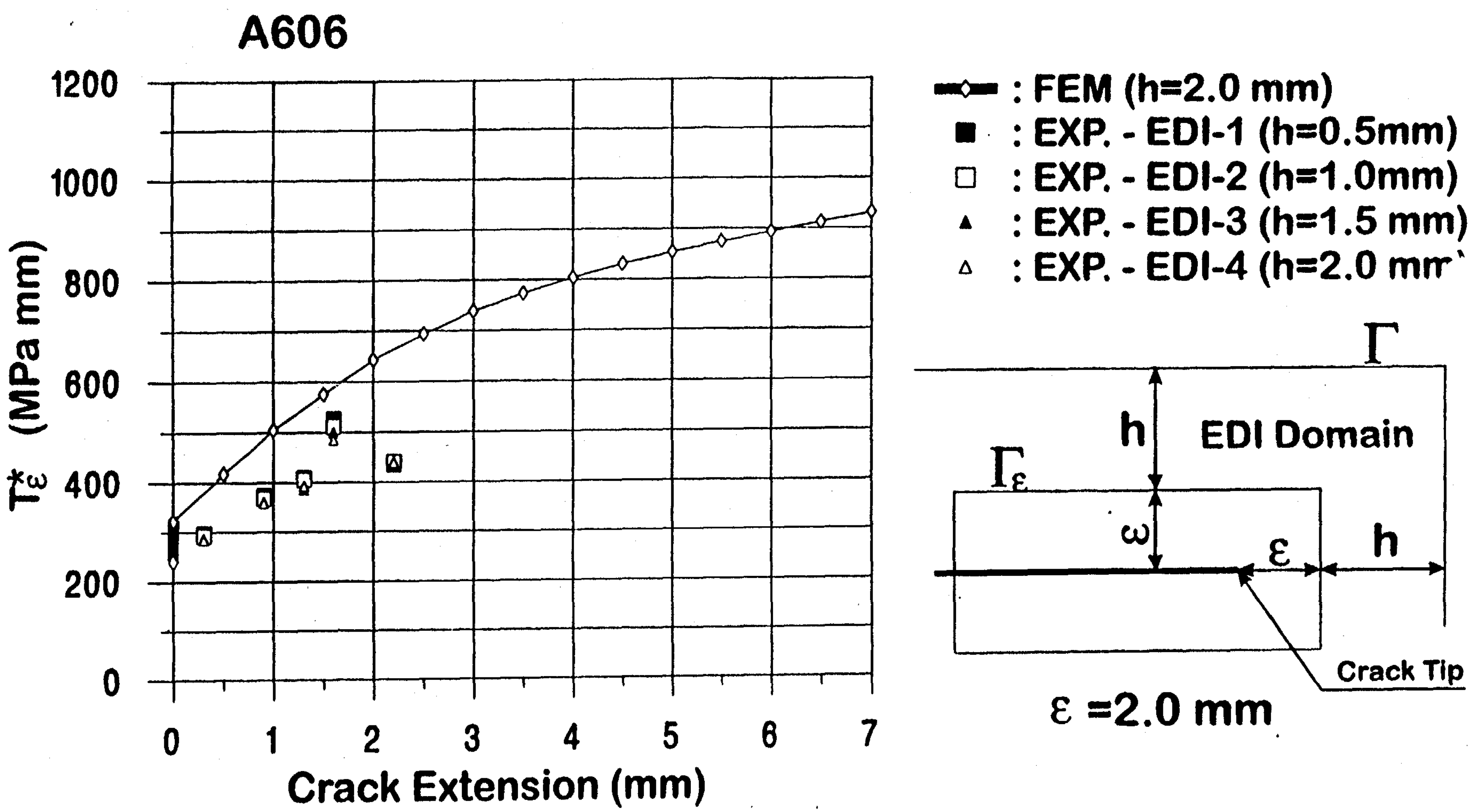
A606
1200
1000
800
600
400
200
0
T^*_ε (MPa mm)
0
1
2
3
4
5
6
7
Crack Extension (mm)
: FEM (h=2.0 mm)
: EXP. - EDI-1 (h=0.5mm)
: EXP. - EDI-2 (h=1.0mm)
: EXP. - EDI-3 (h=1.5 mm)
: EXP. - EDI-4 (h=2.0 mm
Γ
h
EDI Domain
Γ_ε
ω
ε
h
Crack Tip
ε =2.0 mm

Figure 24